A Novel Ortho-Mode Transducer for the 750-1150 GHz Band

by

Siddhartha Sirsi

A Thesis Presented in Partial Fulfillment

of the Requirements for the Degree

Master of Science

Approved November 2014 by the
Graduate Supervisory Committee:

Christopher Groppi, Co-Chair
James Aberle, Co-Chair
Philip Mauskopf

ARIZONA STATE UNIVERSITY

December 2014

ABSTRACT

The design, fabrication and testing of a novel full waveguide band ortho-mode transducer (OMT) for operation from 750-1150 GHz is presented in this dissertation. OMT is a device that separates orthogonal polarizations within the same frequency band. At millimeter and sub millimeter wavelengths, OMTs can achieve precise characterization of the amplitude, spectrum and polarization of electromagnetic radiation by increasing spectral coverage and sensitivity while reducing aperture size, optical spill and instrumental polarization offsets. A fully planar design is implemented with the use of Robinson OMT model along with a planar finline circuit. CST Microwave Studio is used to design and simulate OMT. Existing finline circuits which were fabricated using photolithographic techniques on a thin dielectric substrate were employed. The finline chips are fabricated on a thin (1 μm) SOI substrate with thick (5 μm) gold finline metallization and gold beam leads for chip grounding. The OMT is designed with H plane splits in the through arm and E plane splits in the side arm to comply with the existing machining tools and technique. Computer Numerical Controlled (CNC) machining is used to fabricate the OMT split block. The OMT is tested at Jet Propulsion Laboratory (JPL) using Agilent PNA-X VNA and VDI WR1.0 extension heads. In the future, this OMT design could be a part of a fully integrated dual polarization mixer block, with the input horn, OMT and both mixers fabricated in a single flangeless split block. In Radio Astronomy, integrated dual polarization mixers of this type will increase the signal processing speed by 40%. This type of OMT can also be used for terahertz RADAR and communication purposes.

ACKNOWLEDGEMENTS

I would like to thank my advisor Dr. Christopher E. Groppi for providing the opportunity to work on this project. I could not have accomplished this without your support and guidance. I would also like to thank Dr. James Aberle and Dr. Philip Mauskopf for taking the time to serve as the panel members.

I would also like to thank Matthew Underhill for all the effort he put in fabricating the device parts and Hamdi Mani for painstakingly assembling the entire device.

I would like to thank Dr. Goutam Chattopadhyay for making all the necessary arrangements for my visit to Jet Propulsion Laboratory (JPL) and for his guidance during the testing of the device. Also, I would like to thank Theodore J Reck, JPL for building the test set up and helping me during the testing process.

Finally, I would like to thank my parents and friends for their continued support.

TABLE OF CONTENTS

CHAPTER Page

LIST OF TABLES

Table Page

LIST OF FIGURES

Figure Page

Figure Page

Figure Page

Introduction

1.1 Background

An Orthomode Transducer (OMT) is a device that separates orthogonal polarizations within the same frequency band. In the literature, OMT's are called by various other names such as polarization diplexers, dual-mode transducers, orthomode junctions or orthomode tees. Imaging applications at millimeter and submillimeter wavelengths demand precise characterization of the amplitude, spectrum and polarization of electromagnetic radiation. The use of a waveguide OMT can help achieve these goals by increasing spectral coverage and sensitivity while reducing aperture size, optical spill, instrumental polarization offsets and lending itself to integration in focal plane arrays.

There is an ever increasing need for antenna systems to operate over large bandwidths in almost all applications, from radio astronomy to defense. To increase further the capacity and versatility of the antenna system, dual-polarization operation is often required. With the development of high-performance feed horns capable of dual-polarization performance over bandwidth ratios up to 2.4:1, there is a need to develop an OMT of similar bandwidth performance to match the capabilities of the horn.

With receiver noise temperatures of waveguide-based Superconductor Insulator Superconductor (SIS) and Hot Electron Bolometer (HEB) mixers approaching a few times the quantum limit, further increase in sensitivity can be obtained using dual polarized operation. In radio astronomical applications, the conventional way to separate orthogonal polarizations is the wire grid diplexer, which is quasi optical device that consists of free-standing parallel wires. The polarization with the E-field parallel to the

wires is reflected, while the component orthogonal to the wires is transmitted through. However, the wire grid polarization is large and bulky. If we desire the mixers for both polarization to reside in one cryostat, the wire grid should preferentially be inside the dewar, which correspondingly increases the size of the required dewar. A broadband waveguide based OMT would be a preferable alternative as it would be much smaller and it would be a good match to available high performance dual- polarized broadband corrugated feedhorns.

1.2 Thesis Organization

Chapter 2 consists of brief description of different types of OMT and the reasons supporting the choice of a particular design model. Chapter 3 delves in to the initial design procedure and calculations. CST modeling and simulation is discussed in Chapter 4. Solid Works design is covered in Chapter 5. Chapter 6 deals with the fabrication process. Testing procedure and set up is included in Chapter 7 followed by conclusion.

2 Orthomode Transducer

2.1 Classification

OMTs are classified into three main groups based on symmetry. A device is defined as symmetrical if different transitions causes the dominant mode to generate only symmetrical higher order modes. A device is defined as nonsymmetrical if the dominant mode in addition generates odd symmetrical higher order modes [3].

Class one: The first class represents the simplest and most common approach. It consists of OMTs where a main arm is used for one mode, and an orthogonal side arm for the other mode.

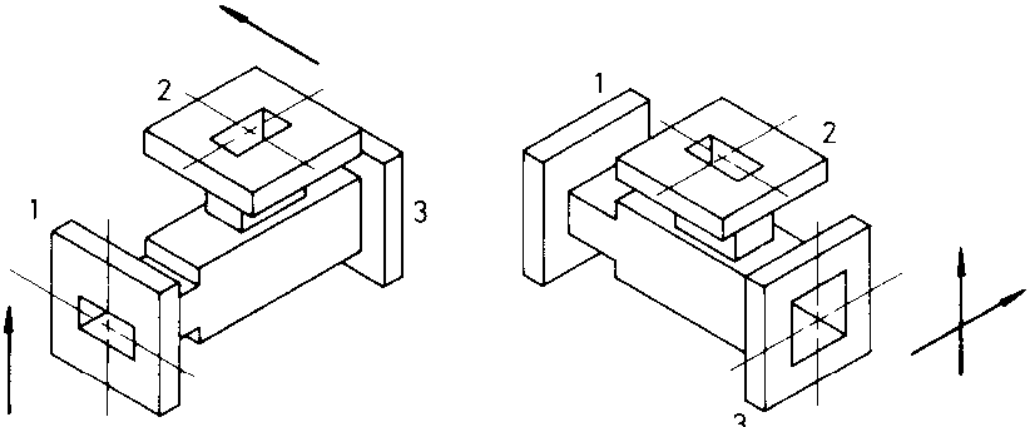

1. Standard OMT(from Schlegel and Fowler[2])

Class Two: Here the side arm is split into two symmetrical parts from the main arm. The mode in the main arm sees a symmetrical device, as it does in class one. It therefore only couples to symmetrical higher modes and cancelling effects lead to a natural broadband

isolation behavior for this mode. In this group the mode in the side arm also sees symmetrical splitting and combining junctions.

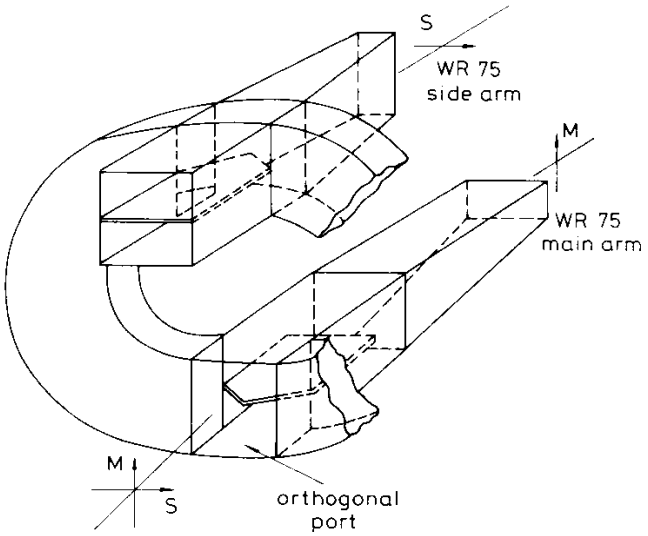

2. OMT with side arm split into H-plane bends(from Brain [4[)

Class Three: Here both the side arms and main arms are split into two symmetrical parts. The splitting junction then forms a turnstile junction. One arm of these OMTs might be split into two symmetrical E-plane bends, while the other arm is split into two symmetrical H-plane bends as in Fig.2.

2.2 Bøifot Design

The design is non planar and consists of two-fold symmetric junction which achieves full waveguide band performance by limiting the excitation of TE_{11} and TM_{11} in the square common-port. The two fold symmetric OMT can be viewed as a variant of the turnstile junction where two of the ports have been folded parallel to the common port. The two ports that form the main arm are separated by a thin septum, combined and transformed to standard height waveguide. For the other polarization, this septum forms a pair of back

to back mitered bends which feed the symmetric side arm ports. The pin number, diameter and location are a compromise between tuning the septum reactance produced in the side arm ports and allowing a low impedance return path for the main arm currents.

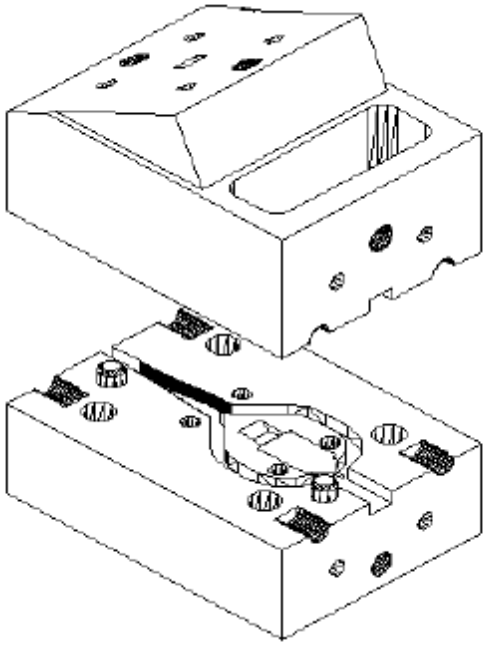

3. WR10.0 OMT Assembly [5]

Recently, Narayanan and Erickson have developed a Bøifot type design replacing the capacitive pins used in previous designs with a capacitive step. This and other refinements make the design far easier to fabricate and make it suitable for scaling to frequencies as high as 1 THz. These waveguide designs offer very low loss, good crosspolarization performance and excellent isolation, but are fundamentally three dimensional.

2.3 Finline OMT

The basic concept of a finline OMT was discussed by Robinson in 1956 [9]. Skinner et al.[10] looked into it in more detail for use in radio telescopes. A finline OMT consists of a square or circular waveguide fitted with diametrically opposite thin tapered metallic fins. The dominant mode electric field parallel to the fins is gradually transformed to a finline mode whose energy is essentially confined to the narrow gap between the fins in the center of the waveguide. This energy then can be removed from the waveguide by curving the finline and bringing it out through the side wall of the guide. The mode polarized orthogonal to the fins passes through the guide virtually unperturbed when the fins are sufficiently thin.

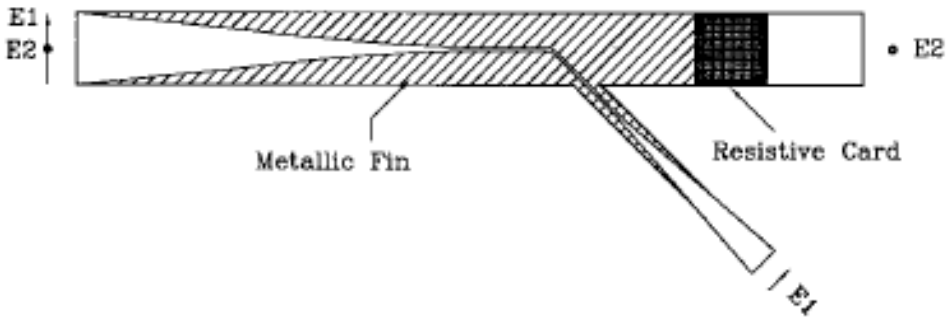

4. Sketch of Finline OMT showing cross sectional view [12].

Two design features have prevented scaling successful Bøifot type OMT designs to higher frequencies: the septum and the capacitive pins used to compensate the septum. The presence of the septum requires capacitive compensation for broadband performance in the side arms. In the newest NRAO design for use in ALMA, these pins are realized as

thin gold wire run through holes in the guide walls. At high frequencies, these pins are nearly impossible to fabricate. The design by Narayanan and Erickson has eliminated these pins in favor of capacitive steps in the waveguide walls. The capacitive steps could be too small to reliably etch at frequencies above 1 THz.

The Finline OMT design proposed by Robinson in 1956 [9] has the potential to be the superior approach for THz applications. This design has been chosen to be optimized for terahertz applications, and fabrication. This device is planar, unlike the Bøifot type designs. A single split block structure contains all the necessary waveguide components, and will allow integration of horns and mixers.

In 2009 Dunning et al.,[22] proposed a planar OMT design for W band. The input section is composed of a square input which is reduced to a smaller square waveguide, followed by a transition to a waveguide with a T-shaped cross section. The polarization separating junction removes one polarization via a mitered bend and allows the other to pass through. Finally each output section consists of a stepped transition to a larger rectangular waveguide. Due to the structural complexities involved, this device is not suitable to be scaled for terahertz frequency design and fabrication using CNC machining.

3 Initial Design

The OMT design consists of two waveguide to finline transitions connected via a 45 degree, half wave radius finline bend. Through-arm transitions from square to full height rectangular waveguide via three section matching transformer, while the full height rectangular side arm uses a mitered 45 degree bend to bring both output guides to the same plane. A waveguide iris is used at the junction between the side and main arms to minimize the effect of the side arm on the horizontal polarization, while not disturbing the finline guide mode.

The OMT will be fabricated using standard CNC machining techniques and not via LASER machining. Thus bends in the H-plane for the through arm and E-plane for the side arms will be incorporated to take into account the radius of the drill bit.

3.1 Performance Criteria

i) Return loss: A number of commercially available quad-ridged horns claim to operate over bandwidth ratios in excess of 3:1. However, this is achieves at the expense of (in part) a return-loss performance which can be as low as 10 dB over part of the band. Such a return-loss performance is unacceptable in many instances, especially so in application to radio astronomy, where it is essential for losses to be kept to a minimum. A return loss of no less than 15 dB is more usual, with close to 20 dB over most of the operating band desirable. This more stringent performance criterion inevitably reduces the bandwidth capability.

ii) Isolation: The isolation between the output ports of the OMT is of importance and a figure of at least 30 dB is considered essential where dual polarization is required.

iii) Cross-Polarization: An important consideration often overlooked in the design of wide-band waveguide components is the excitation of unwanted high-order modes. These are inevitably excited to some degree at the higher frequencies. One of the serious manifestations of unwanted modes is the additional levels of cross-polarization radiated by the horn antenna used in conjunction with the OMT. Thus, another performance criterion in the OMT design is the increase in the cross polar field that can be tolerated over that of the inherent level from the horn alone. A figure of 40 dB is desired.

iv) Insertion Loss: The insertion loss of OMT must be kept to a minimum, with some applications, such as radio astronomy, demanding a figure considerably below 0.5 dB for frequencies in the lower GHz region [10].

v) Bandwidth: Designed for the ALMA 10 band, 787 GHz to 950 GHz

Other criteria, such as ease of manufacture and power handling capabilities will also be of importance under certain circumstances.

3.2 Square to Rectangular Wave Guide Transformer

The dimensions of the square and rectangular waveguide were selected such that they satisfied the bandwidth requirement and were compatible with existing waveguide horn designs.

Square Waveguide: 240 µm by 240 µm

Rectangular Waveguide: 240 µm by 120 µm

The cut off frequency of the waveguide is given by:

$$f_{c(m,n)} = \frac{c}{2\pi\sqrt{\varepsilon_r}} \sqrt{\left(\frac{m\pi}{a}\right)^2 + \left(\frac{n\pi}{b}\right)^2}$$

Where $c = 3 \times 10^8\ m/s,\ \varepsilon_r = Relative\ permittivity$

For TE_{10} mode and $a = 240\ \mu m, b = 120\ \mu m$

$$f_{c(10)} = 625\ GHz$$

Similarly for TE_{20} mode,

$$f_{c(20)} = 1250\ GHz$$

The range of operation is estimated by considering frequency values 10% above $f_{c(10)}$ and 20% below $f_{c(20)}$.

Estimated frequency range of operation: 688 GHz to 1000 GHz

Operating frequency (f) = 829 GHz

The wave number and propagation constant are calculated as below:

$$k = \frac{2\pi}{\lambda} = 17362.53/m$$

$$\beta = \sqrt{k^2 - (\frac{\pi}{a})^2} = 11406.59/m$$

The TE wave impedance can be found as

$$Z_{TE} = \frac{k\eta}{\beta} = 573.8\ \Omega$$

Where $\eta = 377\ \Omega$

The impedance of the rectangular waveguide section is then given by

$$Z_R = \frac{\pi}{2} \times \frac{b}{a} \times Z_{TE} = 450.66\ \Omega$$

Similarly the impedance of the square wave guide is found to be

$$Z_S = 901.32\ \Omega$$

In order to determine the optimum solution for the design of the square to rectangular transition of the through-arm, the following three models were looked at.

3.2.1 Binomial Multisection Matching Transformer

The passband response of a binomial matching transformer is optimum in the sense that, for a given number of sections, the response is as flat as possible near the design frequency.

A three step (N=3) binomial matching transformer was designed using the data from Table1 [11].

	$N=2$		$N=3$			$N=4$			
Z_L/Z_0	Z_1/Z_0	Z_2/Z_0	Z_1/Z_0	Z_2/Z_0	Z_3/Z_0	Z_1/Z_0	Z_2/Z_0	Z_3/Z_0	Z_4/Z_0
1.0	1.0000	1.0000	1.0000	1.0000	1.0000	1.0000	1.0000	1.0000	1.0000
1.5	1.1067	1.3554	1.0520	1.2247	1.4259	1.0257	1.1351	1.3215	1.4624
2.0	1.1892	1.6818	1.0907	1.4142	1.8337	1.0444	1.2421	1.6102	1.9150
3.0	1.3161	2.2795	1.1479	1.7321	2.6135	1.0718	1.4105	2.1269	2.7990
4.0	1.4142	2.8285	1.1907	2.0000	3.3594	1.0919	1.5442	2.5903	3.6633
6.0	1.5651	3.8336	1.2544	2.4495	4.7832	1.1215	1.7553	3.4182	5.3500
8.0	1.6818	4.7568	1.3022	2.8284	6.1434	1.1436	1.9232	4.1597	6.9955
10.0	1.7783	5.6233	1.3409	3.1623	7.4577	1.1613	2.0651	4.8424	8.6110

Table 1. Binomial Transformation Design [11]

The impedances of each step of the binomial transformer are:

Z_1 = 826.36 Ω, Z_2 = 637.33 Ω, Z_3 = 491.53 Ω

The corresponding ‘b’ dimension of each step was calculated using

$$Z = \frac{\pi}{2} \times \frac{b}{a} \times Z_{TE}$$

Thus, b1 = 220 µm, b2 = 170 µm, b3 = 131 µm

The length of each section is calculated as

$$l = \frac{\lambda_g}{4} = 138\ \mu m$$

Where λ_g is the guide wavelength and is given by

$$\lambda_g = \frac{2\pi}{\beta}$$

3.2.2 Chebyshev Multisection Matching Transformer

In contrast with binomial transformer, the multisection Chebyshev matching transformer optimizes bandwidth at the expense of passband ripple. Compromising on the flatness of the passband response leads to a bandwidth that is substantially better than that of the binomial transformer for a given number of sections. A three step (N=3), Υ_m=0.05 Chebyshev matching transformer was designed using the data from Table 2 [11].

	$N=2$				$N=3$					
	$\Gamma_m = 0.05$		$\Gamma_m = 0.20$		$\Gamma_m = 0.05$			$\Gamma_m = 0.20$		
Z_L/Z_0	Z_1/Z_0	Z_2/Z_0	Z_1/Z_0	Z_2/Z_0	Z_1/Z_0	Z_2/Z_0	Z_3/Z_0	Z_1/Z_0	Z_2/Z_0	Z_3/Z_0
1.0	1.0000	1.0000	1.0000	1.0000	1.0000	1.0000	1.0000	1.0000	1.0000	1.0000
1.5	1.1347	1.3219	1.2247	1.2247	1.1029	1.2247	1.3601	1.2247	1.2247	1.2247
2.0	1.2193	1.6402	1.3161	1.5197	1.1475	1.4142	1.7429	1.2855	1.4142	1.5558
3.0	1.3494	2.2232	1.4565	2.0598	1.2171	1.7321	2.4649	1.3743	1.7321	2.1829
4.0	1.4500	2.7585	1.5651	2.5558	1.2662	2.0000	3.1591	1.4333	2.0000	2.7908
6.0	1.6047	3.7389	1.7321	3.4641	1.3383	2.4495	4.4833	1.5193	2.4495	3.9492
8.0	1.7244	4.6393	1.8612	4.2983	1.3944	2.8284	5.7372	1.5766	2.8284	5.0742
10.0	1.8233	5.4845	1.9680	5.0813	1.4385	3.1623	6.9517	1.6415	3.1623	6.0920

Table 2. Chebyshev Transformer [11]

The impedances and the corresponding ‘b’ dimension of each step of the Chebyshev transformer are:

Z_1 = 785.46 Ω, Z_2 = 637.33 Ω, Z_3 = 517.138 Ω

b1 = 209 µm, b2 = 170 µm, b3 = 138 µm

3.2.3 Hecken Taper

For a given taper length, the Klopfenstein impedance taper is optimum in the sense that the reflection coefficient is minimum over the passband. But Klopfenstein taper has discontinuities at the taper ends which introduce unwanted effects in certain applications. The Hecken impedance function is not optimum in the Klopfenstein sense, but achieves matching without impedance steps. For any bandwidth and maximum magnitude of reflection coefficient in the passband, the Hecken taper is only slightly longer than the optimum taper. Detailed derivation of the Hecken impedance function is discussed in Hecken [18]. The MATLAB code used to calculate the finite impedance steps and the corresponding waveguide dimensions is developed based on the code given in W. Grammer [19]

3.3 Finline Design

The finline tapers are of simple exponential form $a_0 e^{zl}$, where a_0 is half the b dimension of the waveguide and l is taper length. The taper length was chosen to be 550 μm, as the best compromise between matching and loss. The detailed design methodology is discussed in G. Chattopadhyay & J. E. Carlstrom [12].

4 Design using CST Microwave Studio

The OMT design was carried out using Computer Simulation Technology (CST) Microwave Studio (MWS). CST MWS is based on the finite integration (FI) method, which is a one to one translation of Maxwell's equation into a discrete space formulation without simplification or specialization. The FI method works explicitly in the time domain and hence a full broadband simulation can be performed in one single solver run. Transient solver, a general purpose 3D EM simulator was used to run simulations. Besides the specific capabilities in time domain, the transient solver also delivers broadband frequency domain results like S-parameters. These simulations can be performed with an arbitrarily fine frequency resolution without extra computational cost, thus avoid missing single resonance inside the spectrum.

4.1 Binomial Multisection Matching Transformer

The previously calculated values for the dimensions of each step of the transformer was used to design the model. Bends in the E-plane with a radius of 60 µm were added to accommodate for the endmill diameters. The built in optimizer was used to optimize the geometry.

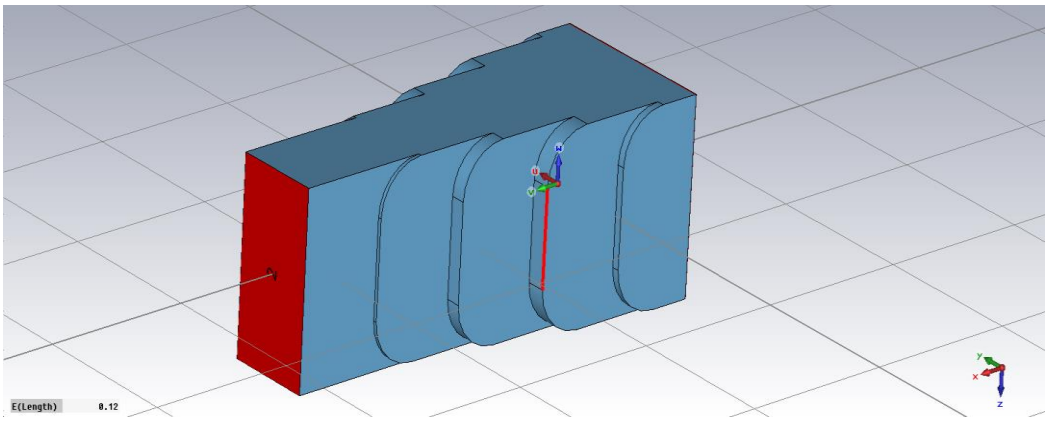

5. Binomial Multisection Matching Transformer

The corresponding S_{11} Parameter was plotted.

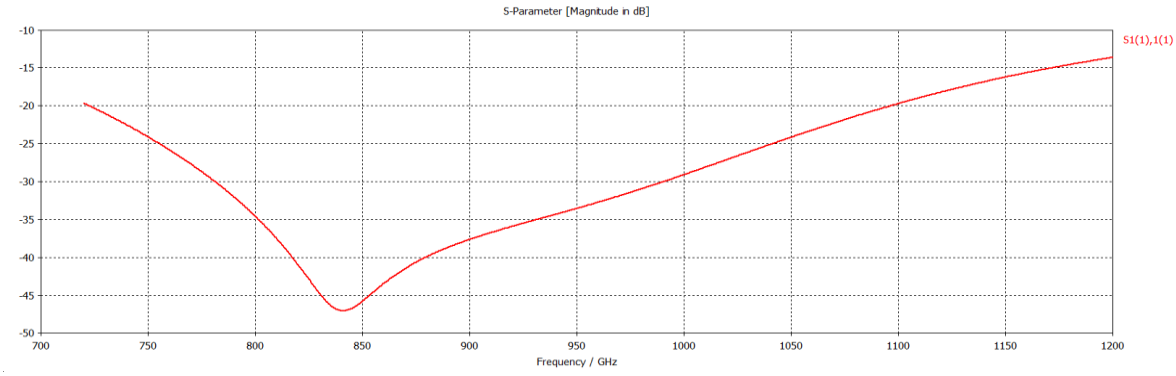

6. S_{11} Parameter- Binomial

The optimized design was then incorporated in the OMT model.

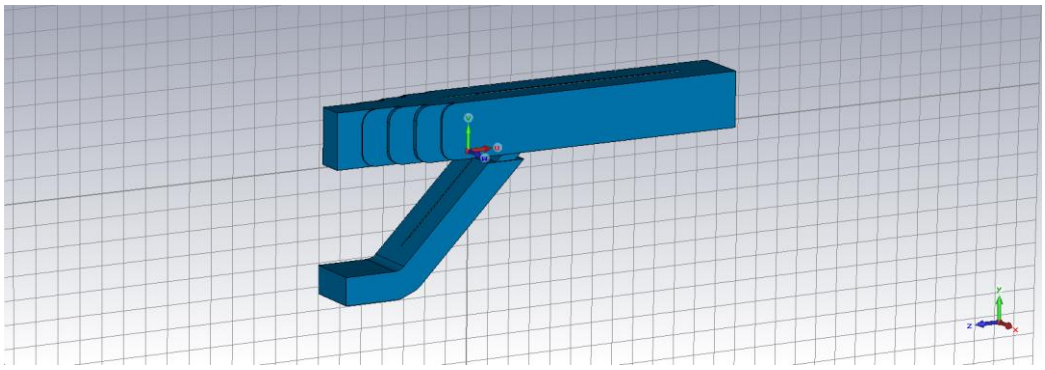

7. OMT with Binomial Multisection Matching Transformer

The corresponding through arm and side arm return loss were then plotted.

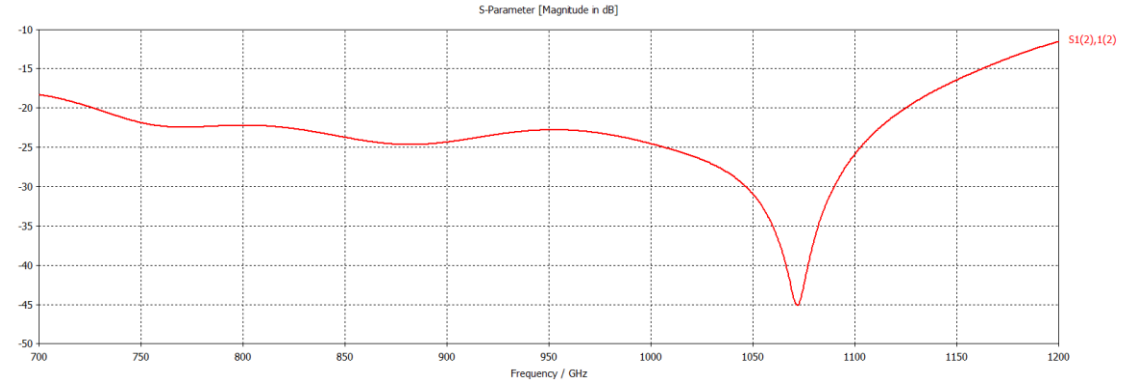

8. S_{11} Parameter for the through arm-Binomial

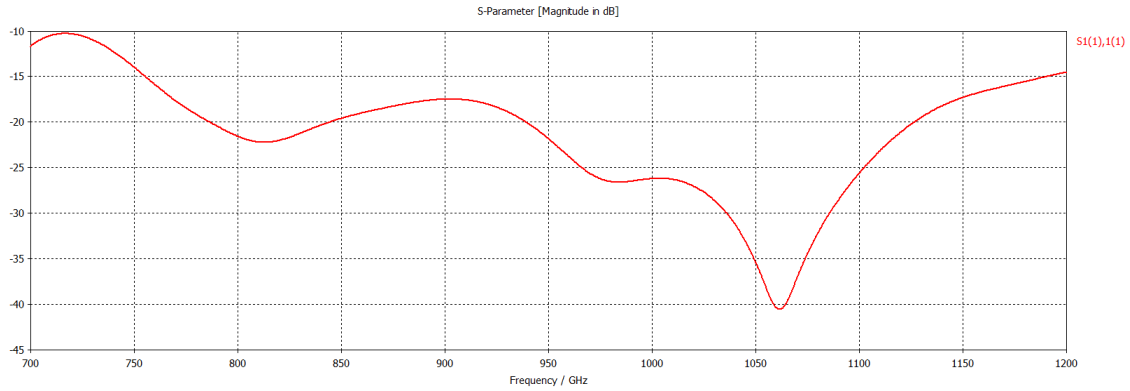

9. S_{11} Parameter for the side arm-Binomial

4.2 Chebyshev Multisection Matching Transformer

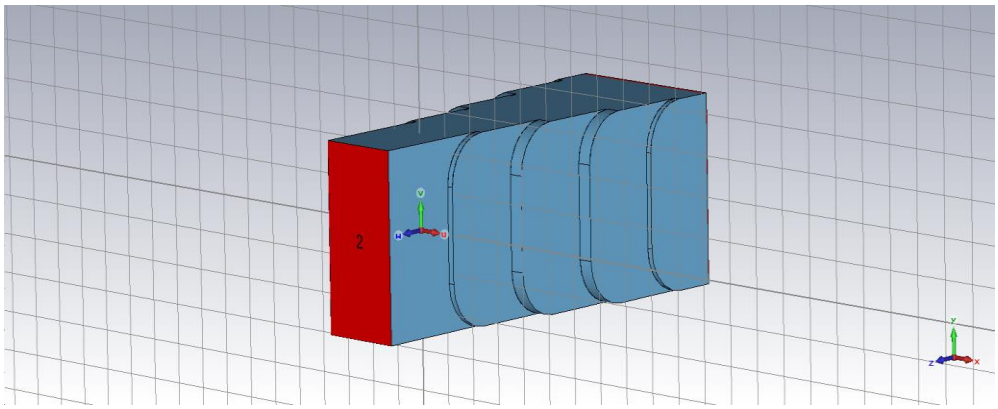

10. Chebyshev Multisection Matching Transformer

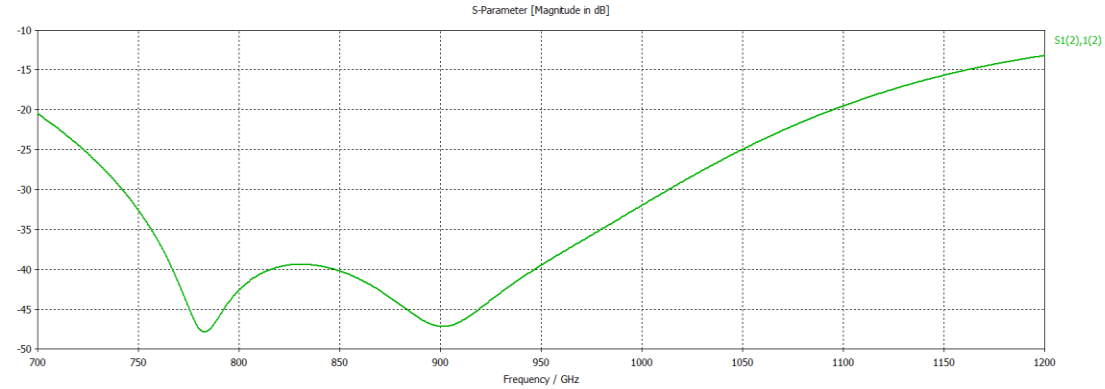

11. S_{11} Parameter-Chebyshev

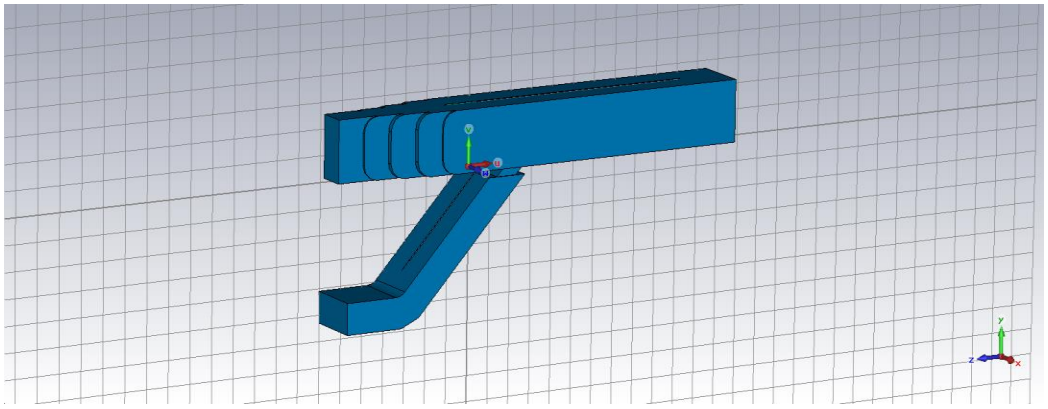

12. OMT with Chebyshev Multisection Matching Transformer

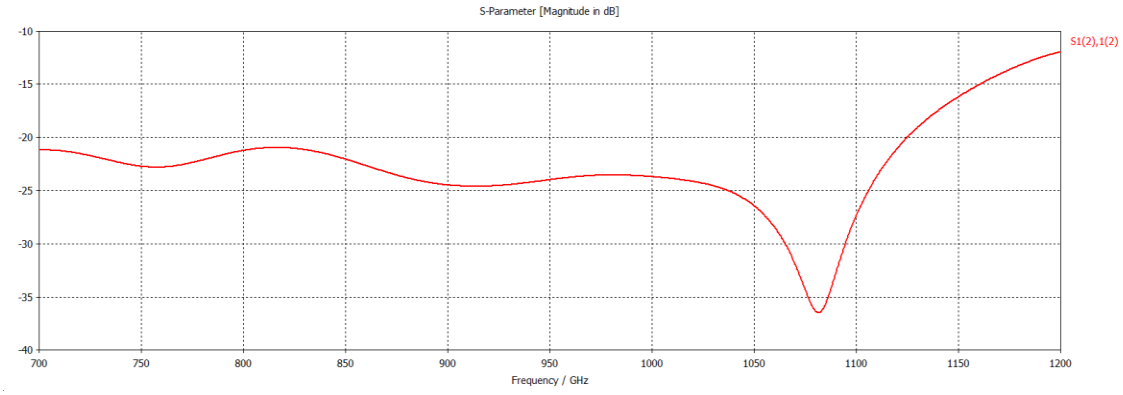

13. S_{11} Parameter for the through arm- Chebyshev

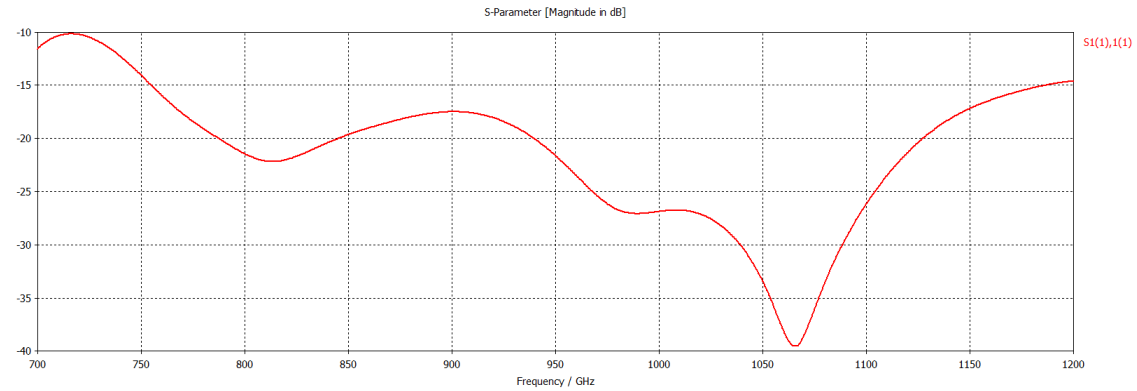

14. S_{11} Parameter for the side arm- Chebyshev

4.3 Hecken Taper

The set of dimensions generated using the MATLAB code was used to design the taper.

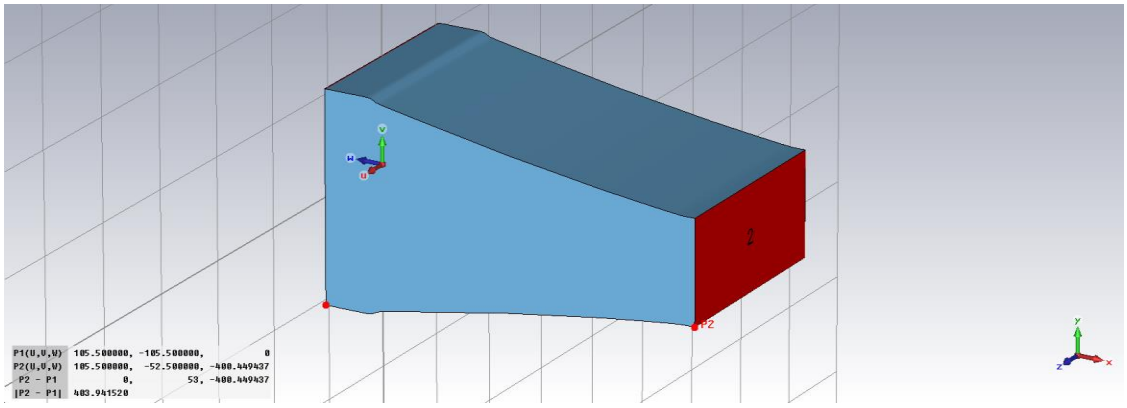

15. Hecken Taper

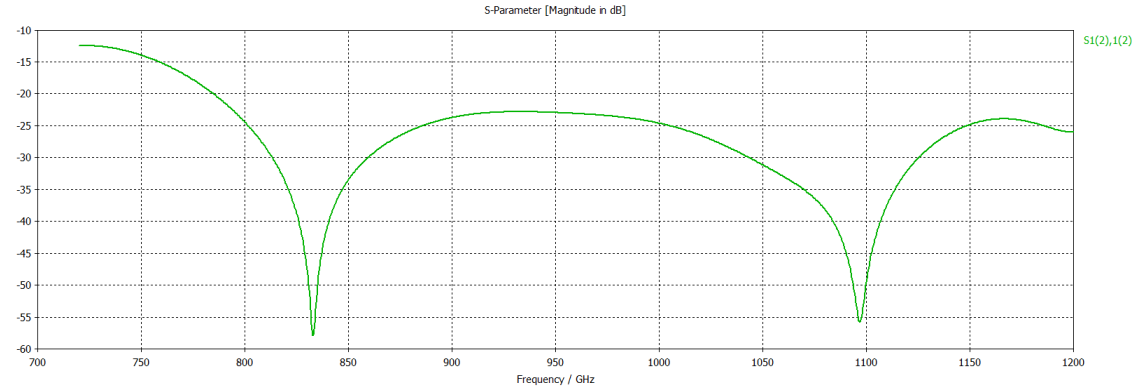

16. S_{11} Parameter- Hecken

Hecken Taper was not considered for the final design for the following reasons:

1) Hecken impedance function generates a near optimum length taper for a set minimum reflection co-efficient value. For this OMT, the length of the square to rectangle transition is not a design criterion.

2) Binomial or Chebyshev matching sections are much easier to fabricate by CNC machining techniques than Hecken taper.

4.4 Comparison between Binomial and Chebyshev Multisection Matching Transformers

The following table compares the return loss in the side arm of the Binomial and Chebyshev multisection transformers.

Return Loss (dB)	Type	Frequency (GHz)								
		780	800	820	840	860	880	900	920	950
	Binomial	19.14	21.55	22.01	20.33	18.99	18.04	17.49	18.01	21.82
	Chebyshev	19.07	21.45	22.01	20.41	19.02	17.99	17.50	20.07	21.62

Table 3. S_{11} Parameter for side arm

The following table compares the return loss in the through arm of the Binomial and Chebyshev multisection transformers.

Return Loss (dB)	Type	Frequency (GHz)								
		780	800	820	840	860	880	900	920	950
	Binomial	22.40	22.23	22.50	23.27	24.20	24.68	24.36	23.56	22.80
	Chebyshev	22.14	21.24	20.98	21.53	22.66	23.81	24.49	24.59	23.99

Table 4. S_{11} Parameter for through arm

Binomial multisection matching transformer performs slightly better than the Chebyshev transformer over the desired bandwidth. Hence, Binomial transformer is used in the final design.

4.5 Iris Design

The waveguide iris at the junction connecting the through arm and side arm is optimized to improve the response of the side arm. The waveguide iris is designed so as to minimize the effect of the side arm on the horizontal polarization, while not disturbing the finline

guide mode. The performance of the through arm is sacrificed to improve the side arm response.

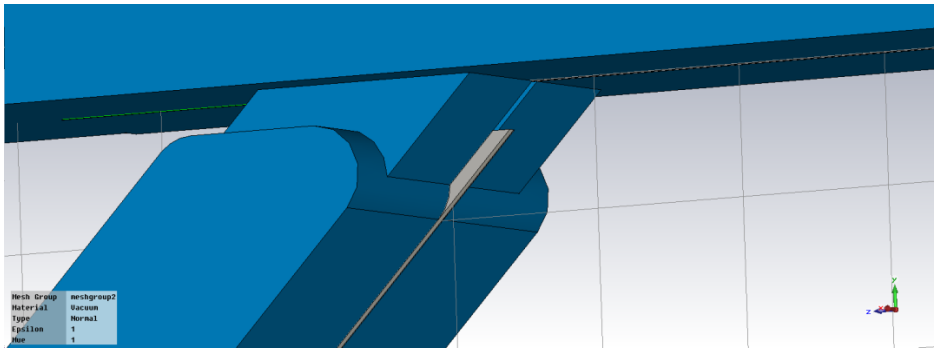

17. Waveguide Iris

4.6 Final Design

The optimized binomial multisection matching transformer and the iris is incorporated in the final design. The through arm has bends in the H plane. The higher order modes wget burnt up in the resistive card at the end of finline. The uncoated silicon substrate at the front portion of the finline acts a transition from waveguide to finline.

The bends in the waveguide are designed to comply with standard micromachining techniques. LASER micromachining is not employed in the fabrication of this OMT.

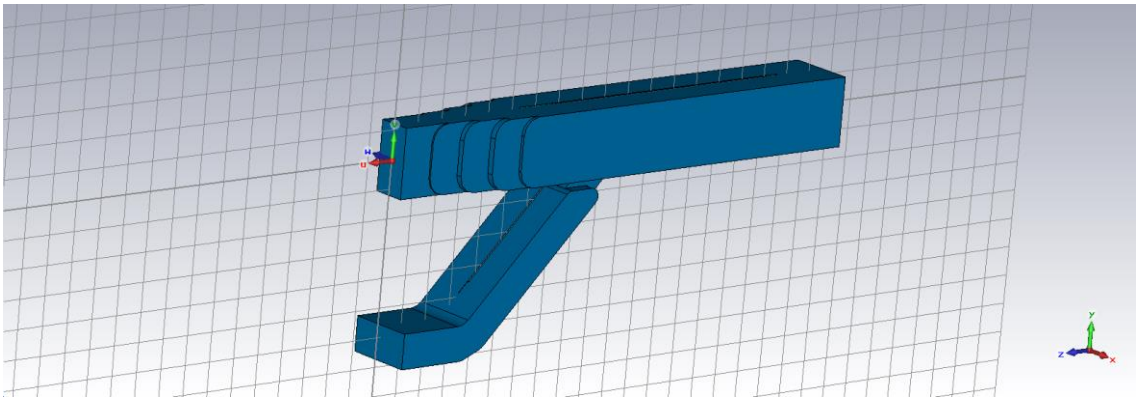

18. OMT- Final Design

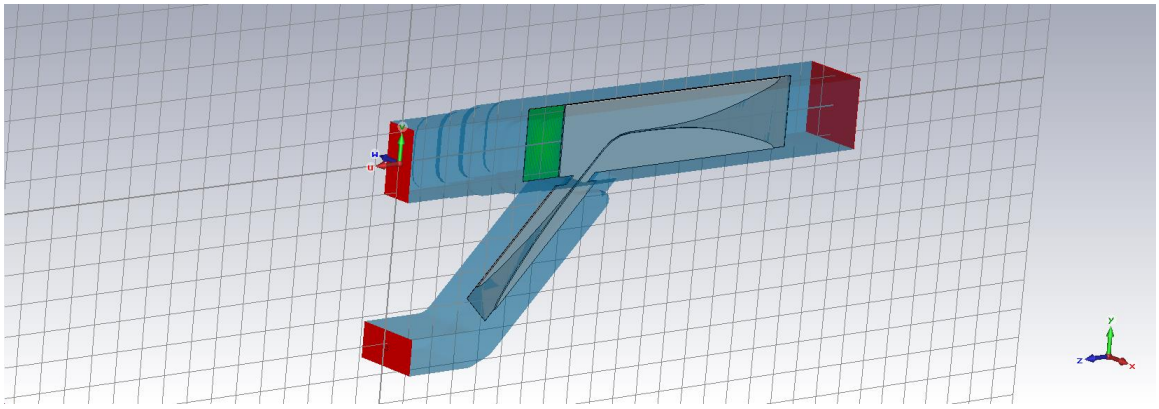

19. OMT- Integrated Finline Circuit

4.7 Simulation Results

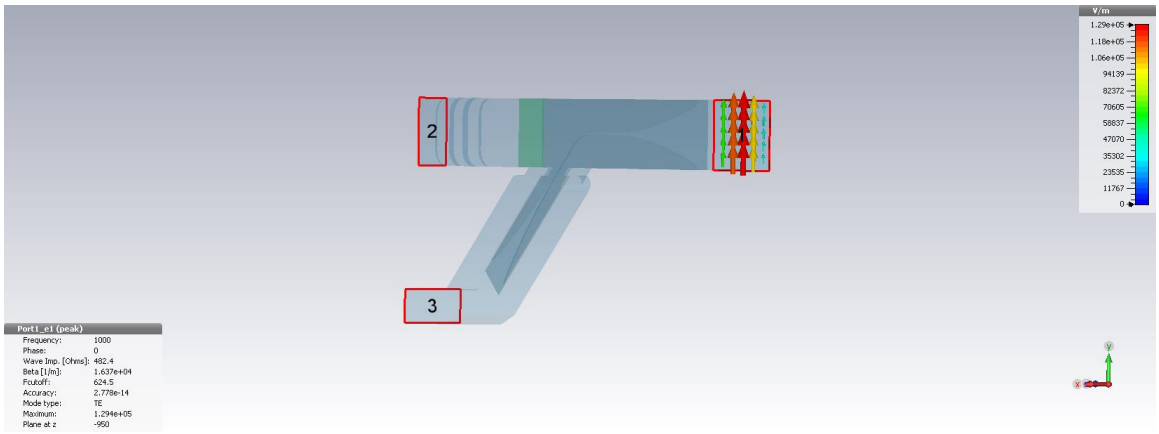

20. E1 Field Excitation for Port 1

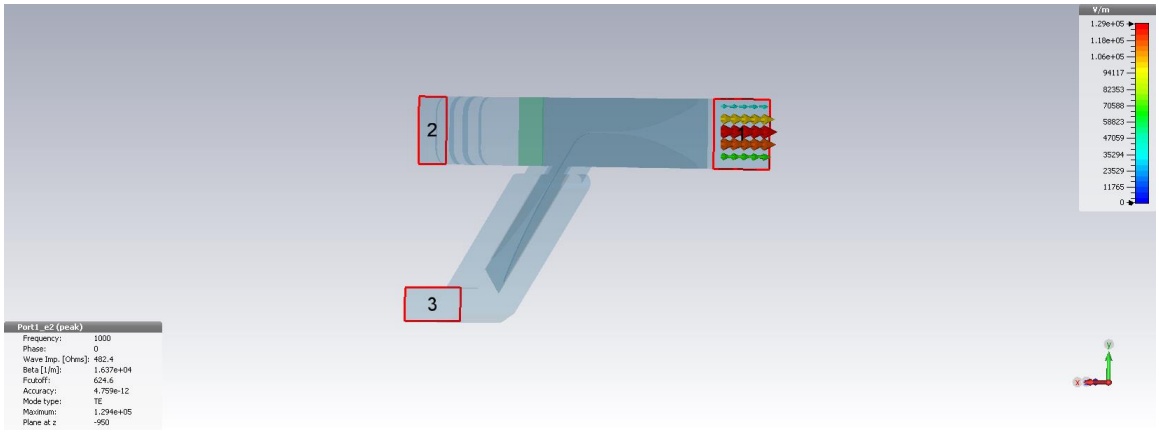

21. E2 Field Excitation for Port 1

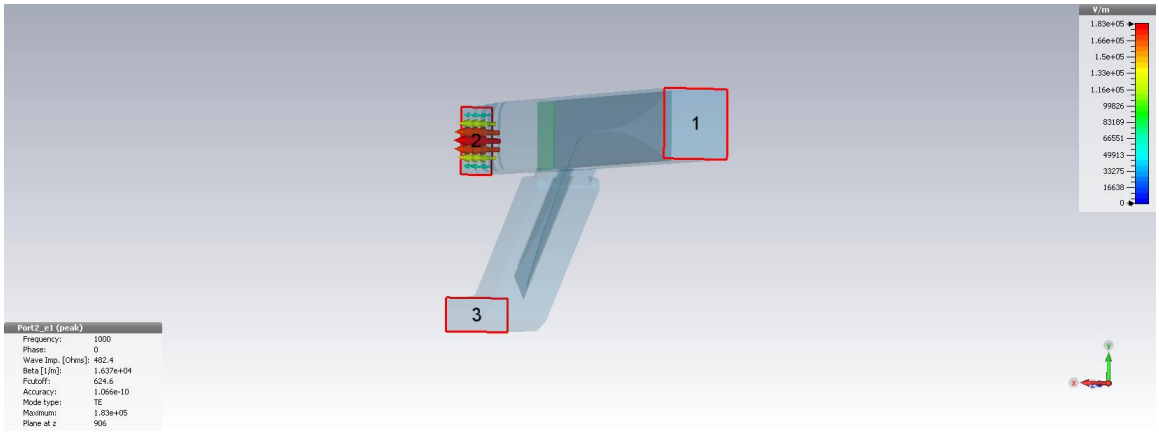

22. E Field Excitation for Port 2

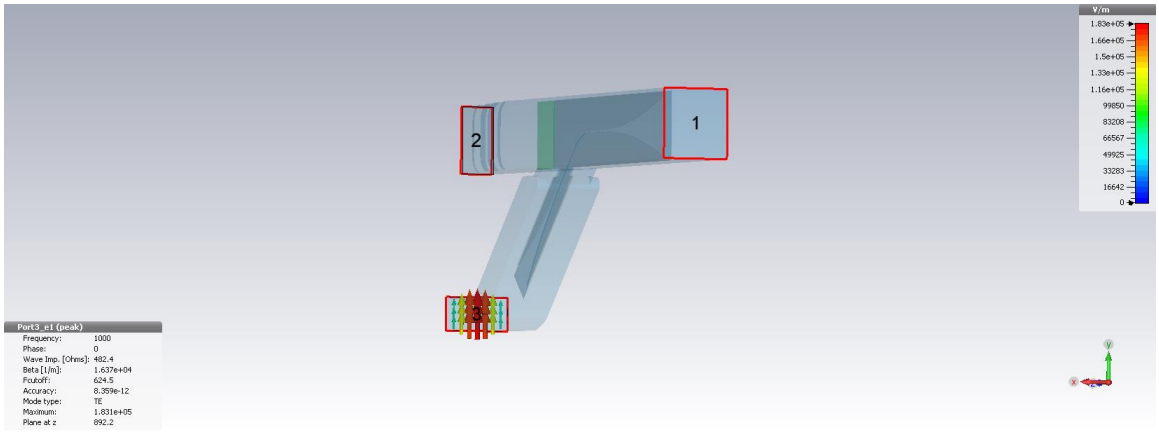

23. E Field Excitation for Port 3

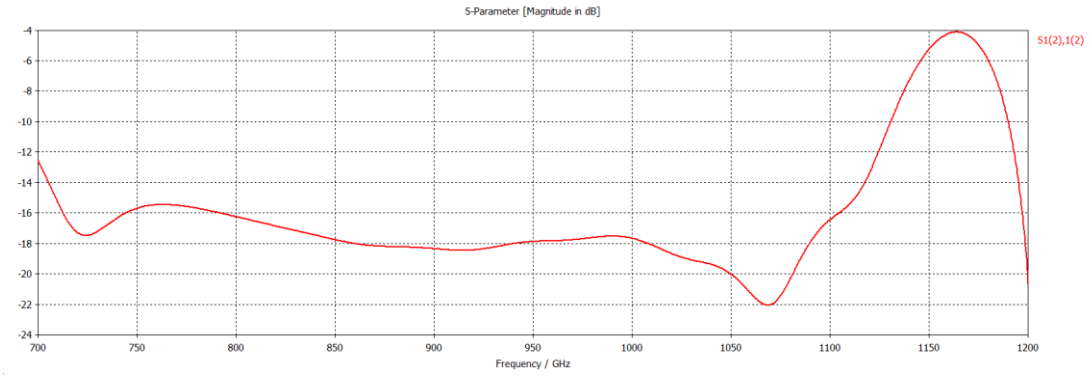

24. Return loss for the through arm- Port 2

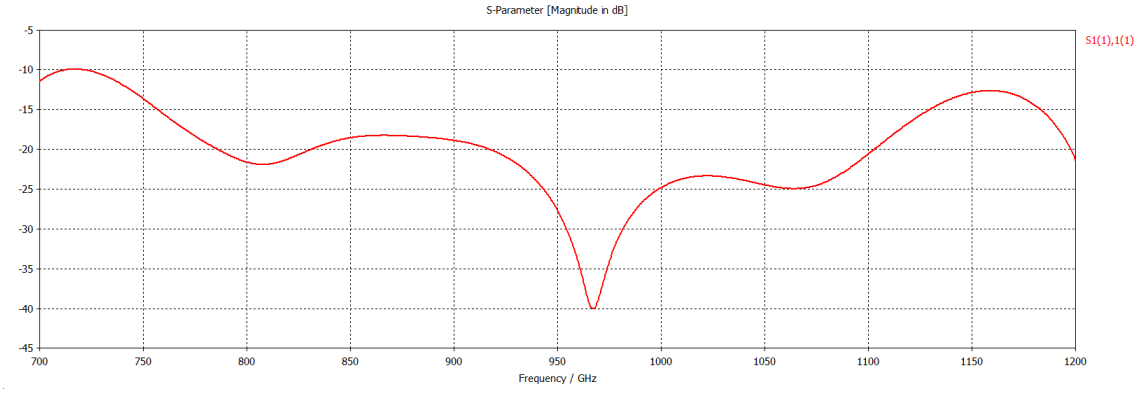

25. Return loss for the side arm- Port 3

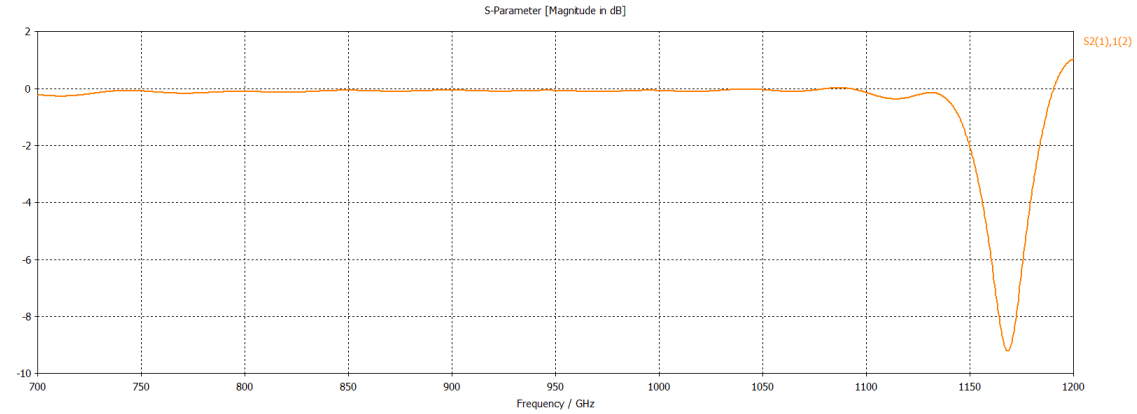

26. Insertion loss for the through arm- Port 2

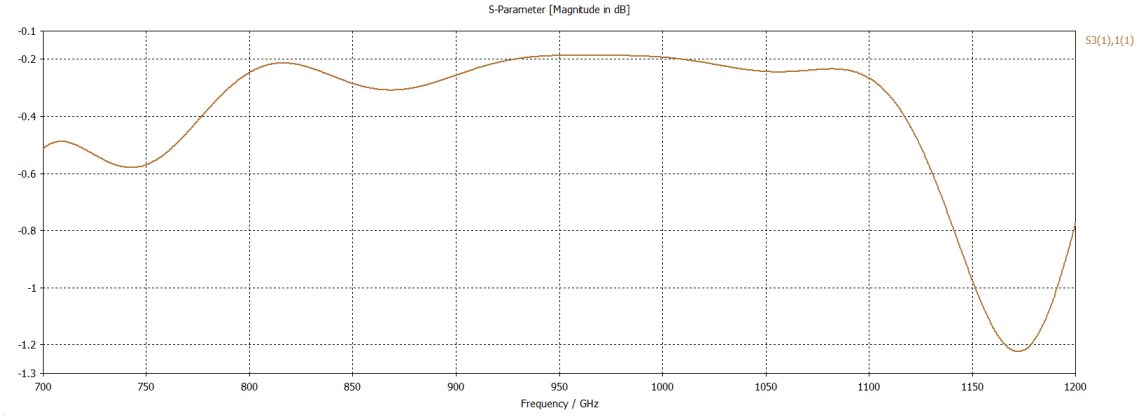

27. Insertion loss for the side arm- Port 3

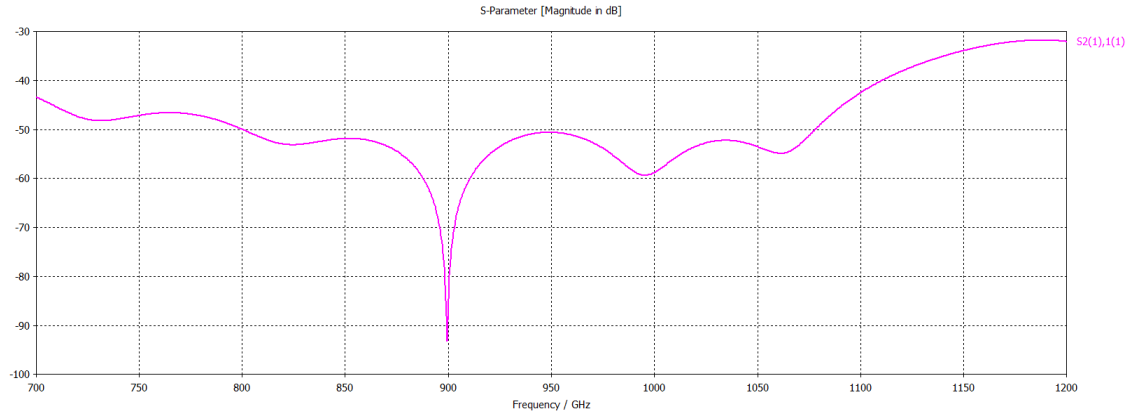

28. Crosspolarization for the through arm- Port 2

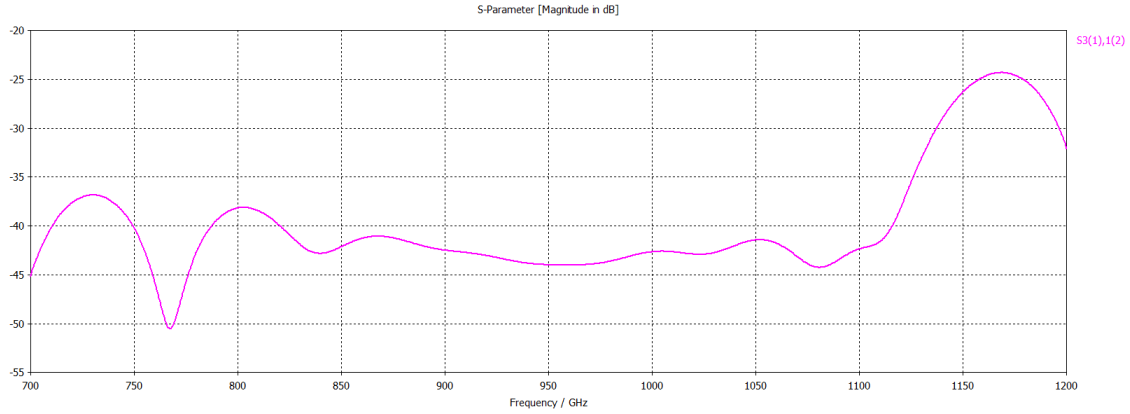

29. Crosspolarization for the side arm- Port 3

5. Design using Solidworks

After optimizing and finalizing the design in CST MW, the next step was to design the OMT in Solidworks. Two different designs were created based on the pre-existing finline chip models. The two finline chips are identical in performance but differ in external structural dimension.

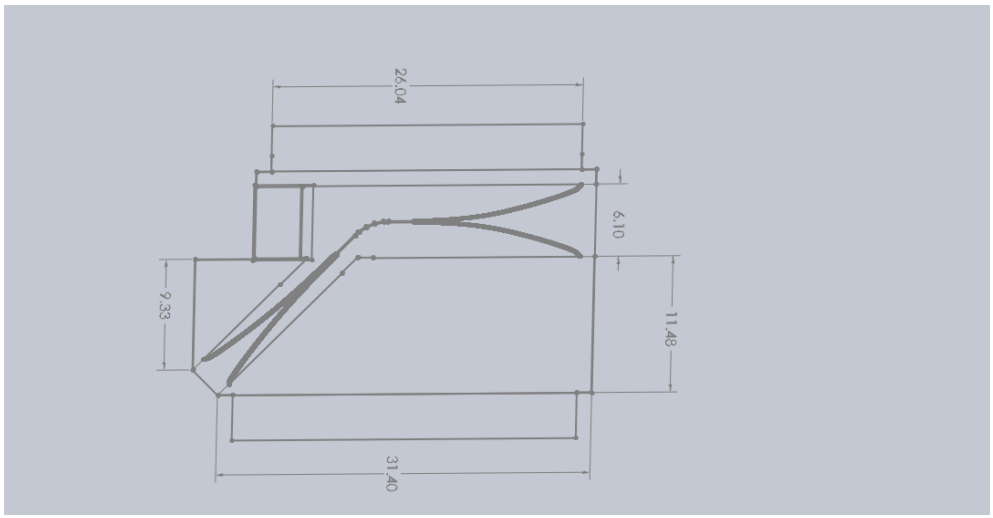

30. Sketch of Finline Chip- Large

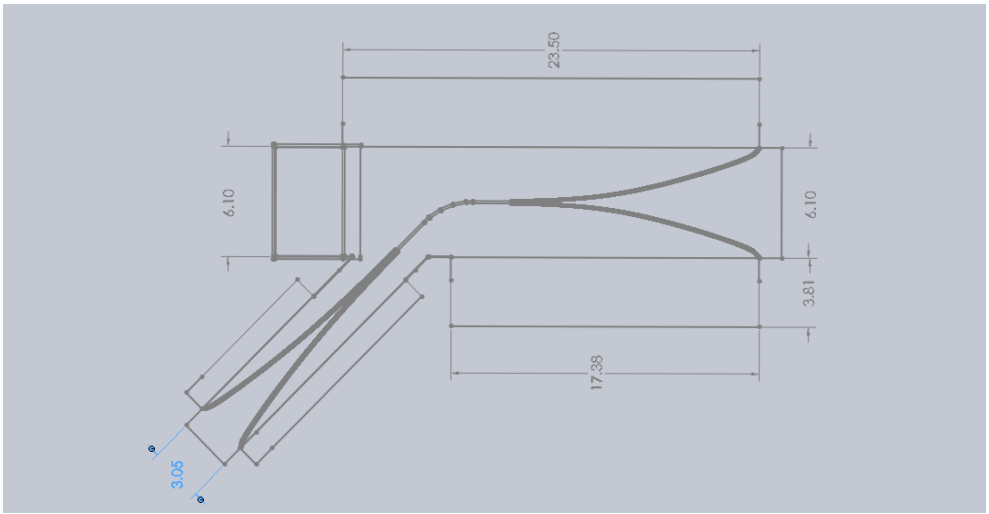

31. Sketch of Finline Chip- Small

All the dimensions are in millimeter (mm).

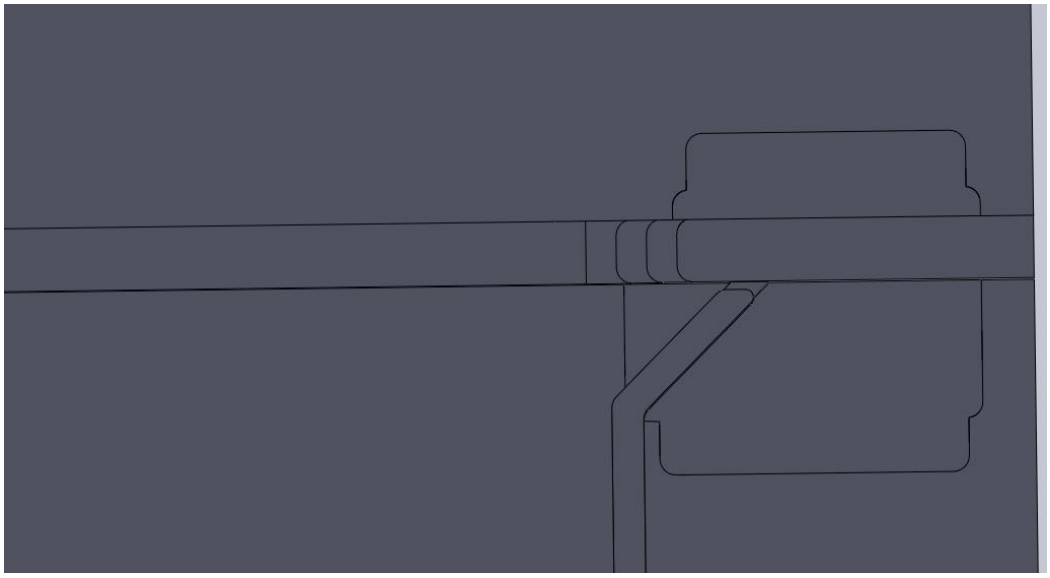

32. OMT-Large Chip Model

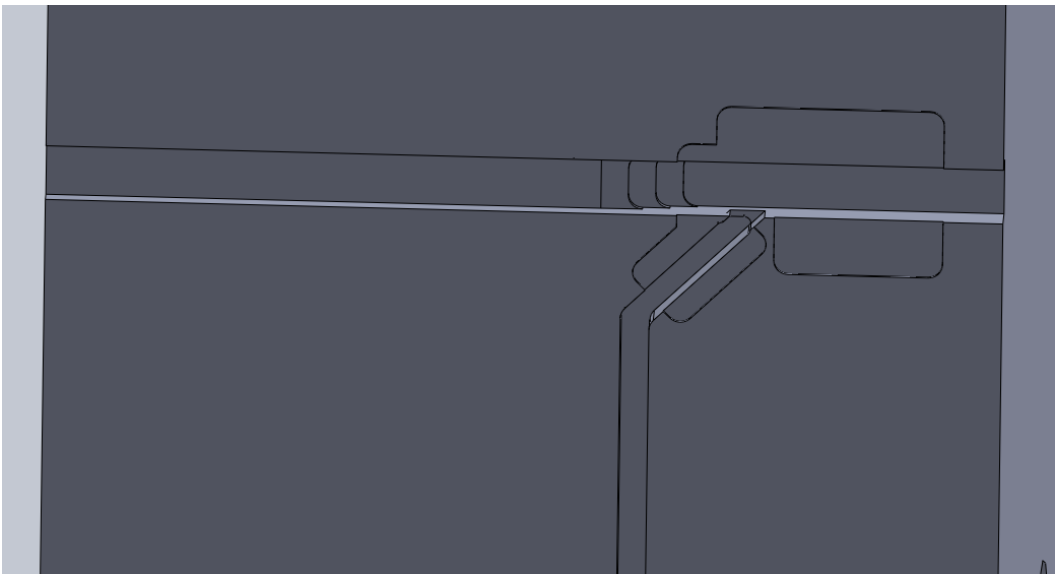

33. OMT-Small Chip Model

The finline chip is 0.005 mm thick. The cut for housing the finline chip is 0.01 mm deep. This is done to position the finline centrally in the waveguide and provide clearance for the beam leads and conductive epoxy used in assembly. Gaps in the block cannot be tolerated because of the H-plane split for one polarization.

The OMT block is 24 mm long and 12.10 mm thick. At the widest part it is 24.32 mm and 4 mm wide at its narrowest part. The dimensions were chosen so as to accommodate 3 I-72 Tapped holes, 4 1/16 Dowel holes, 1 4-40 Tapped hole and 1 2-56 Tapped hole. The test structure is designed with the mitered bend reversed to make the two arms perpendicular to facilitate the addition of output horns.

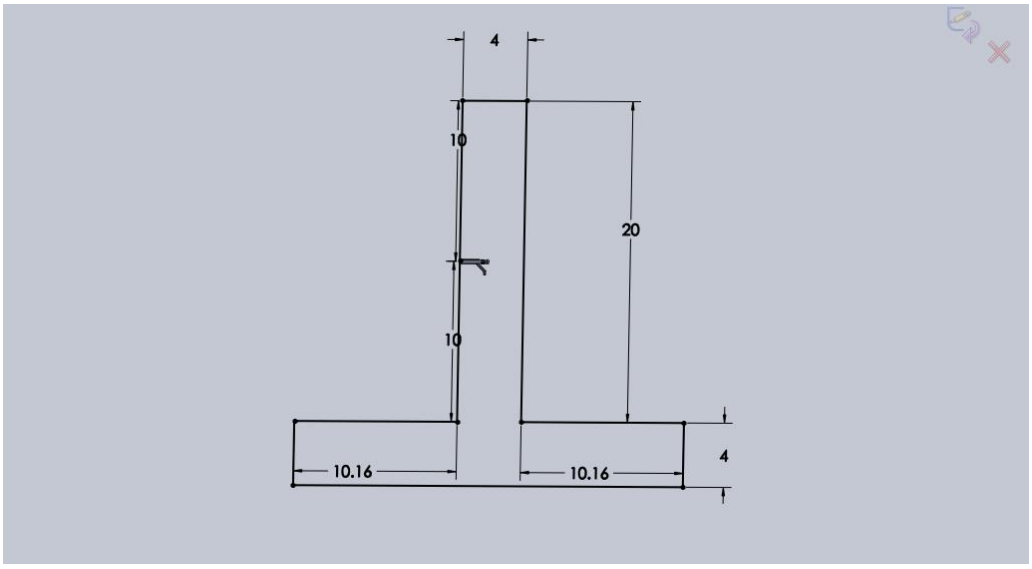

34. Sketch of OMT Block (All dimensions are in mm)

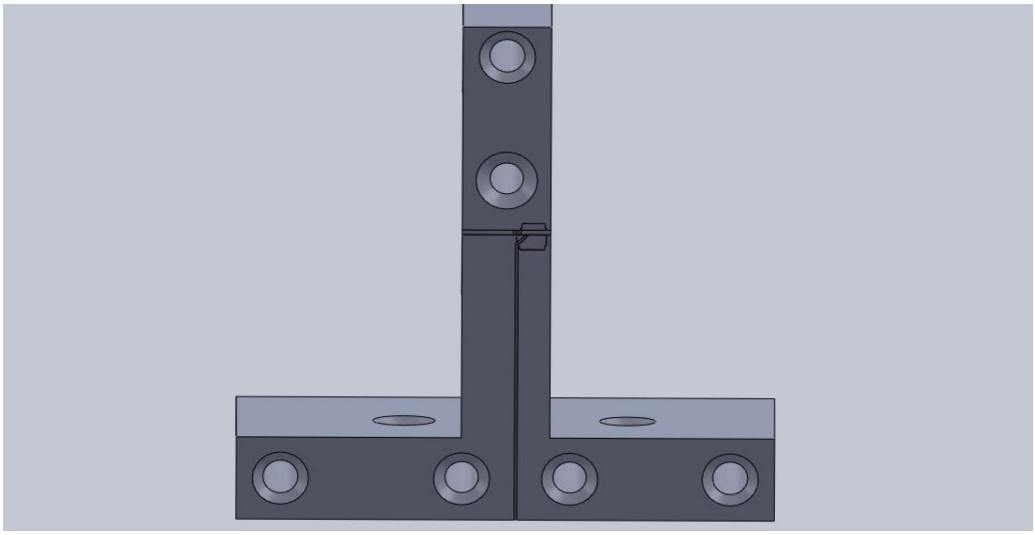

35. OMT-Split Block

The standard UG-387 waveguide flange is used as it has symmetric hole configuration. The flange can be rotated 90 degrees about its central axis to fit both the full height rectangular output and the side arm output.

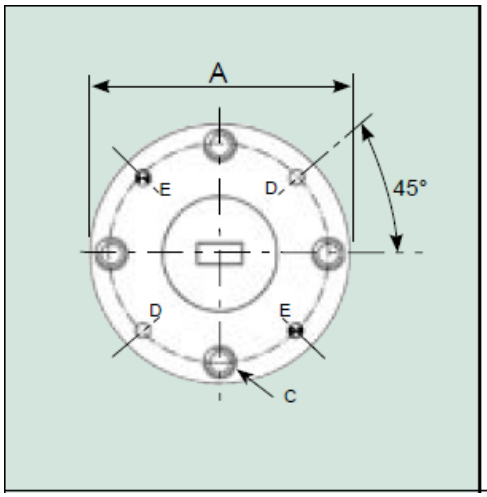

Flann Standard Flanges

WG26 R740 WR12
UG-387/U (MIL-F-3922/67B-009)

Holes C .....4 x 4-40 UNC-2B
Holes D.....2 x 1.65 dia
Holes E.....2 x dowels 1.549/ 1.562 dia x 4 projection
All Holes on 14.29 PCD
A 19.05

Source: Waveguide and Flange Data, www.Flann.com

36. UG-387 Flange Data (All dimensions are in mm)

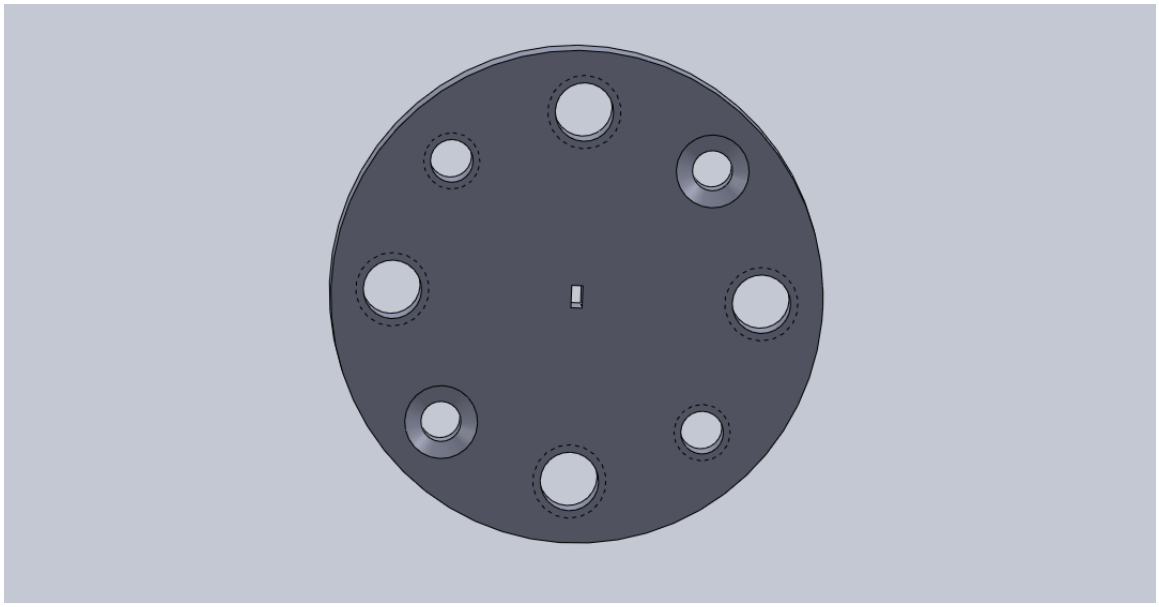

37. UG-387 Flange

The VDI WR1.0 extension heads used at the input port to mate with the network analyzer have rectangular ports. Hence a linear rectangular to square waveguide transformer is designed. The transformer is 25.40 mm long. The performance of the transformer is not critical to the output response of the OMT as the response of the transformer will be de-embedded from the final result thus providing a better estimate of the standalone response of the OMT.

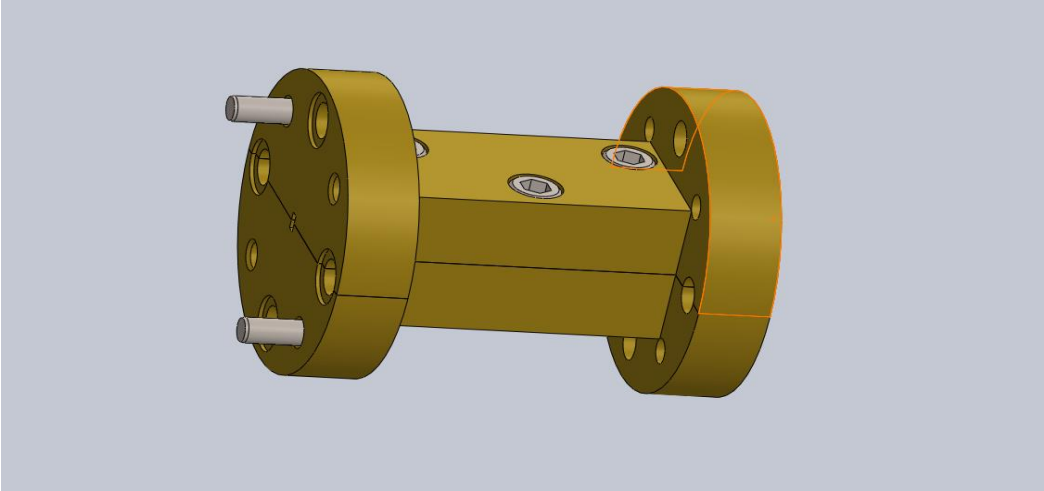

38. Rectangle to Square Waveguide Transformer

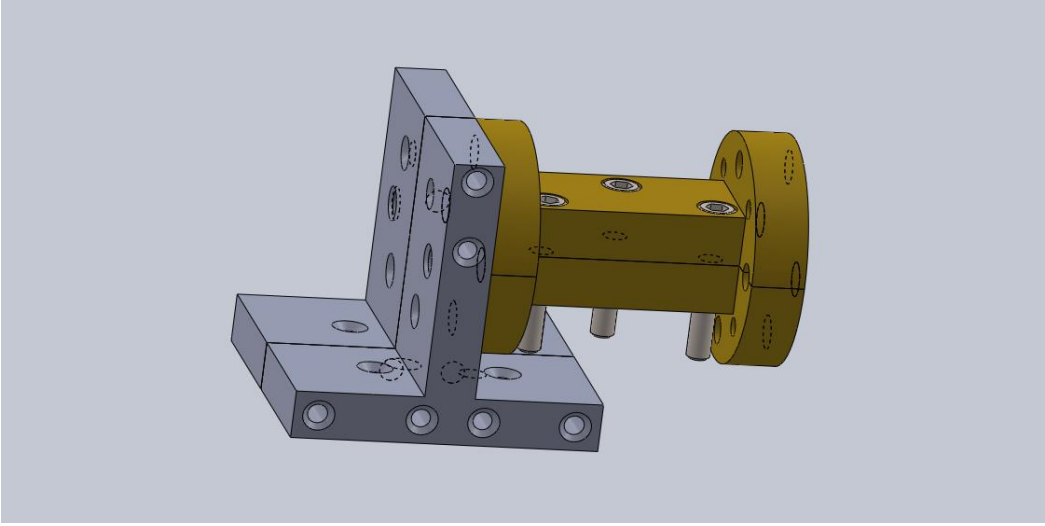

39. Final Assembly

6. Fabrication

6.1 Finline

The finline chip has been fabricated using photolithography on a 1 μm thick SOI substrate.

The use of silicon as a substrate material allows easy realization of the resistive card at the end of the finline. A palladium-gold film with a surface resistivity of 12.5 Ω/□ was deposited on the thin silicon substrate to realize the resistive card. Beamleads are used to ground the device to the block. Beamleads are thin, freestanding metallic tabs fabricated on a substrate that is later etched away. They are thick enough to act as handles for manipulating the structure and offer very good RF grounding performance [1].

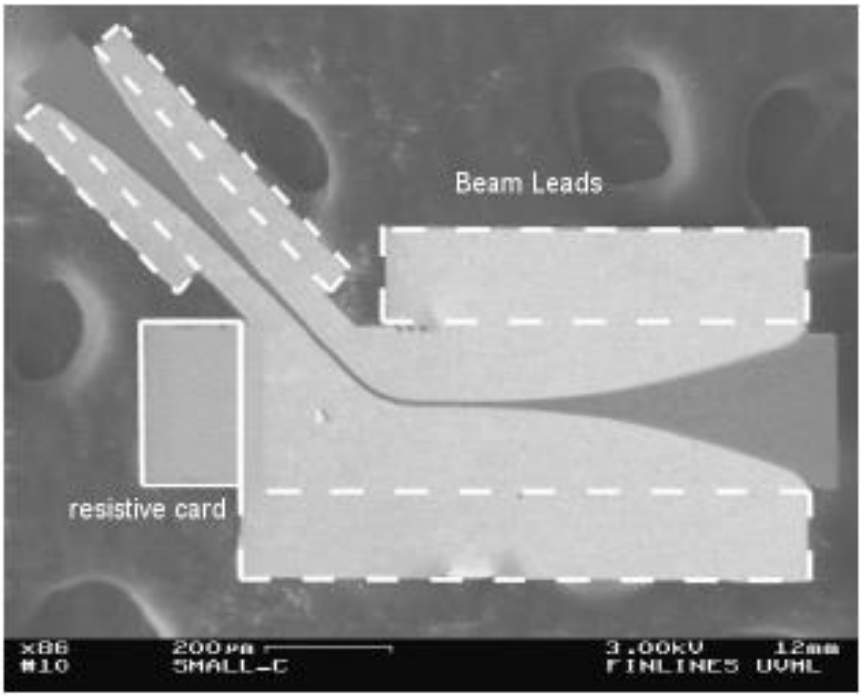

40. SEM image of a finline chip fabricated at the University of Virginia [1].

During assembly, a beam lead device is placed in a split-block waveguide structure, suspended by the beam leads. When the split-block is assembled, the gold beam leads are

typically crushed between the block halves providing grounding. For this design, the beam leads are secured with Epotek H20E conductive epoxy, and are housed in 10 μm deep pockets to ensure the beamlead thickness does not generate a gap between the block halves. A gap could result in resonances in band for the H plane polarization. Beam lead devices are used extensively in the multipliers used in the Hershel HIFI LO system, as well as many modern SIS and HEB detector designs. SOI technique allows silicon membranes thinner than 1 μm to be produced. The thin membrane is attached to a carrier wafer. After fabrication of the structure, the backside carrier wafer is released from the thin membrane. Silicon membranes are fairly flexible, and are much easier to handle than quartz wafers of same thickness. The finline chip is a straightforward fabrication task compared to SIS junction; only a single gold metallization layer needs to be deposited on the substrate. The finline has been defined using standard photolithographic processes on the SOI wafer, using thick photoresist techniques. A 1:1 aspect ratio of the finline gap width to metallization thickness is realizable with these techniques. SEM and interferometric microscope imaging show that the microchip fabricated conform to all the design dimensions to better than 5%

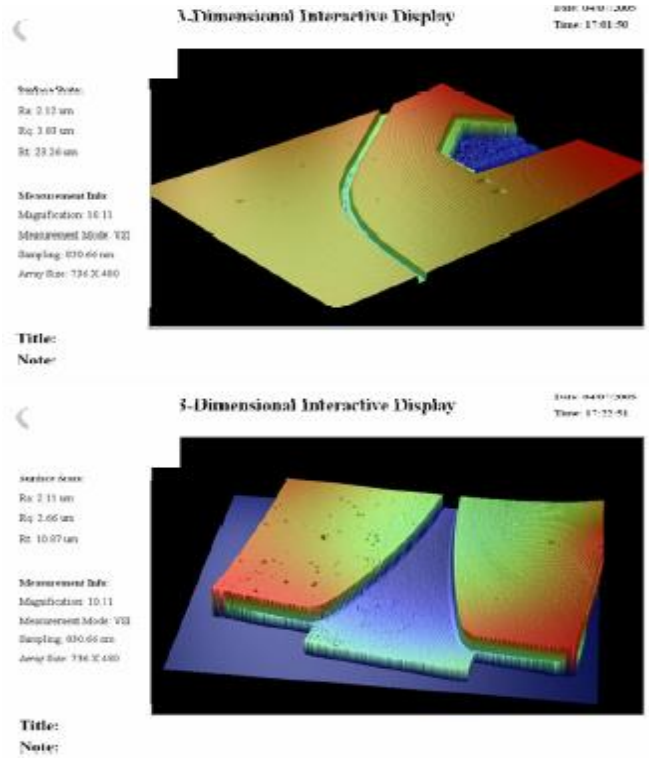

41. Veeco interferometric microscope images of SOI finline chip [1].

6.2 OMT

Computer Numerically Controlled (CNC) machining of splitblock waveguide circuits has become the primary method of constructing terahertz waveguide circuits. The majority of these circuits have been made on traditional CNC machining centers or on custom-made laboratory machining systems. At both the University of Arizona and Arizona State University, techniques for machining splitblock waveguide circuits using purpose-built ultrahigh precision CNC machining centers designed for micromachining have been developed. These systems combine the automation of a traditional CNC machining center, including a high capacity toolchanger, workpiece and tool metrology systems and a large work volume, with the precision of custom laboratory systems. The systems at ASU is built by Kern Micro and deliver typical measured dimensional accuracies of 2-3

microns. Waveguide surface finish has been measured with a Veeco white light interferometric microscope to be Ra~75 nm. Tools of sizes between 25 microns and 10mm are available, with toolchanger capacities of 24-32 tools. The automated toolchanger and metrology systems allow a metal blank to be machined into the final part in one machining cycle, including both micromachining operations and traditional machining operations. This allows for perfect registration between all block features, in addition to very short cycle times. Even the most complicated blocks have machining cycle times of no more than a few hours. Workpiece and tool metrology systems also allow for fast setup times and straightforward part re-work. In addition, other high-throughput techniques such as palletization are enabled for the simultaneous manufacture of large numbers of blocks [20].

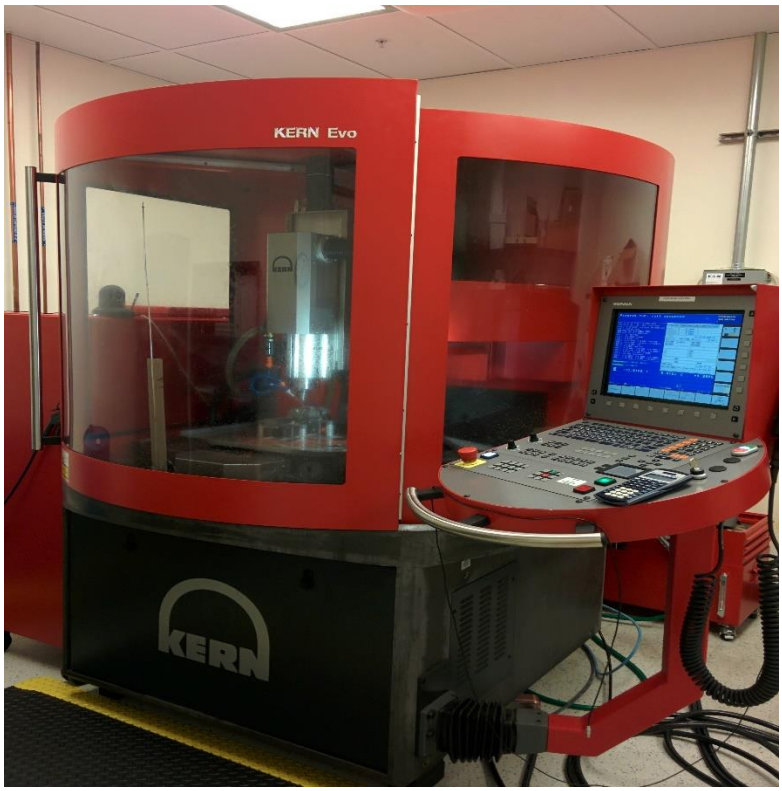

42. Kern Model 44

6.3 Assembly

The finline chip is secured in the slot using Epotek H20E conductive epoxy. The two halves of the split blocks are then assembled together. The entire assembly is placed on a heating pad for 15 min at 250 F. The epoxy hardens and holds the finline in position. The split blocks are separated and the finline chip is inspected to make sure that it has set in the right position.

43. Finline Chip inside the OMT

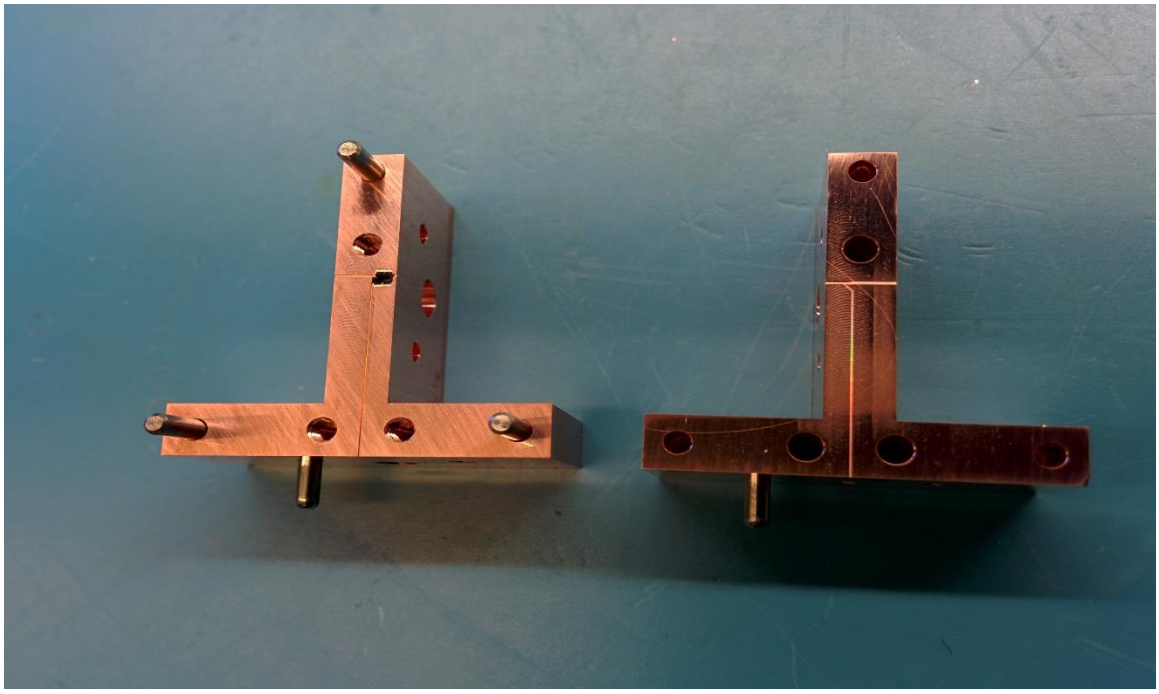

44. OMT split blocks

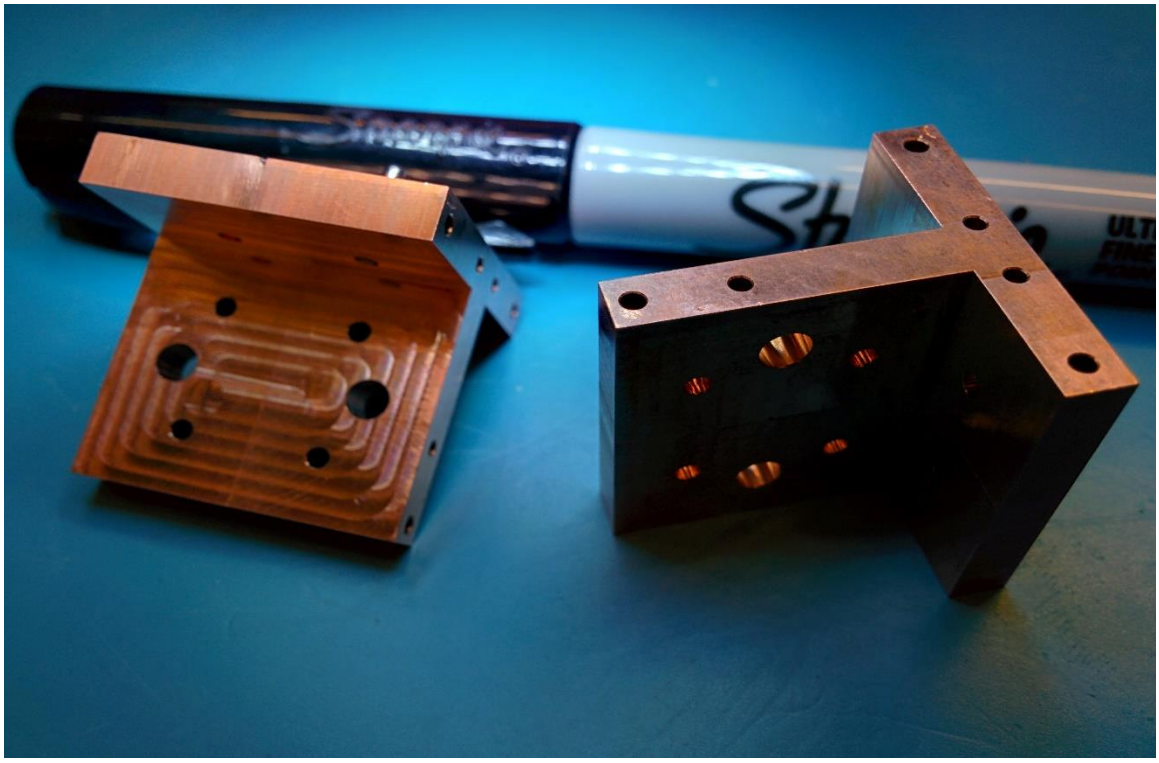

45. Assembled OMT

7. Testing

7.1 Instrumentation

Agilent PNA X Series Microwave Network Analyzer: PNA X with mm wave module has an operating range from 10 MHz to 1.05 THz. It consists of two internal signal sources, signal combiner, S-parameter and noise receivers, pulse modulators and generators and a flexible set of switches and RF access points all with a single set of connections to the device under test (DUT)

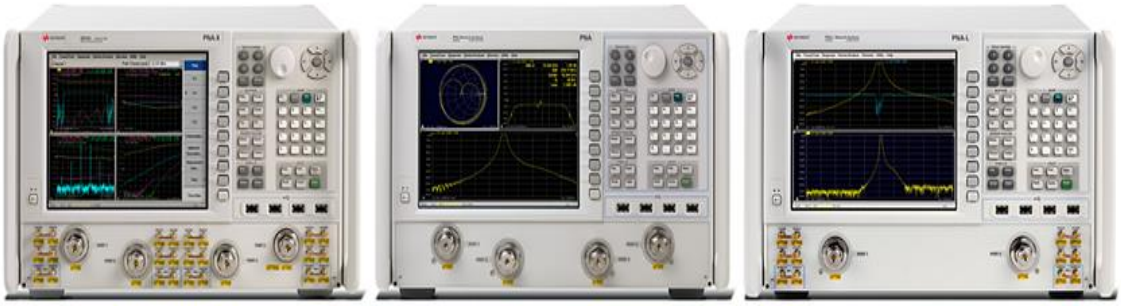

Source: www.keysight.com

46. Agilent PNA-X

VNA Extender- VDI Model WR1.0-VNAX: The WR1.0 has an operating range from 750-1100 GHz.

Specifications:

- Dynamic Range: 60 dB typical at 10Hz BW
- Dynamic Range: 40 dB minimum at 10Hz BW
- Magnitude Stability: ±1 dB
- Phase Stability: ±15°

- Typical Test Port Power: -35 dBm
- Test Port Input Limit (dBm, saturation/damage): -20/13
- Directivity: 30 dB
- Typical Dimensions: 8 x 5 x 3 inches
- Options available:
- Increased Cable Length
- Waveguide Based Calibration Kit

Source: www.vadiodes.com

47. VNA Extender- VDI Model WR1.0-VNAX

7.2 Test Set Up

The OMT was tested at JPL (Jet Propulsion Laboratory) using a Vector Network Analyzer (VNA) consisting of a Agilent PNA-X Network Analyzer and submillimeter-wave OML test set extensions. The VNA was calibrated at the WR1.0 rectangular

waveguides outputs of the extension heads using two-port calibrations with WR1.0 calibration kit. The calibration procedure was used to remove systematic instrumental effects and to calibrate out the response of the instrument up to the chosen calibration planes. Additional measurements of the two pairs of identical back-to-back transitions allowed to calibrate out their individual losses and to derive the S-parameters of the OMT at the physical ports of the device [21]. A picture of the test setup is shown below.

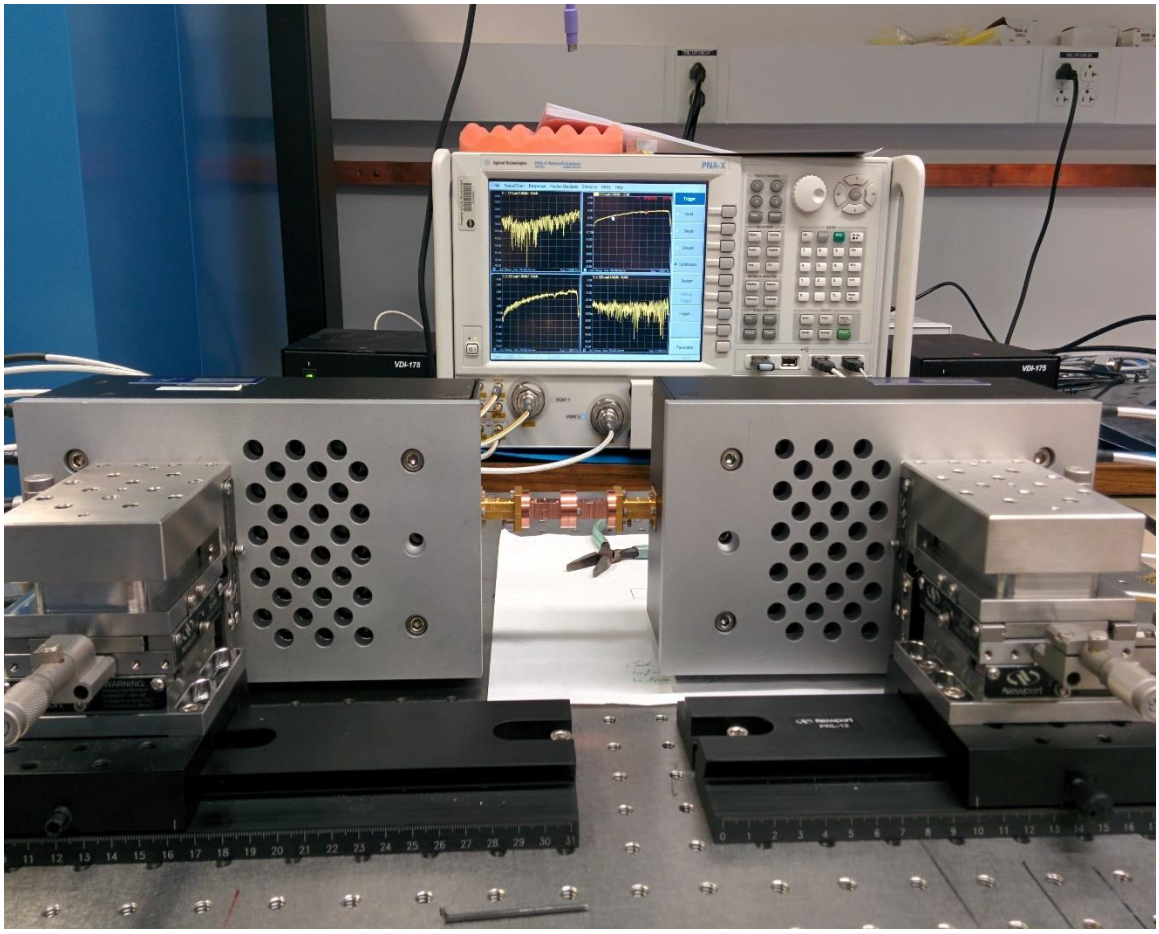

48. Test set up for measuring identical back to back transition

For Pol 2 transmission measurement, the square waveguide input of the OMT was attached to the WR1.0 waveguide port of the network analyzer through the WR1.0 waveguide-to-square waveguide transition. The WR1.0 waveguide output of the OMT was attached to the second WR1.0 waveguide port of the analyzer through a straight section of WR1.0 employing UG387 flange. The side arm waveguide of the OMT was terminated with a matched WR1.0 waveguide load.

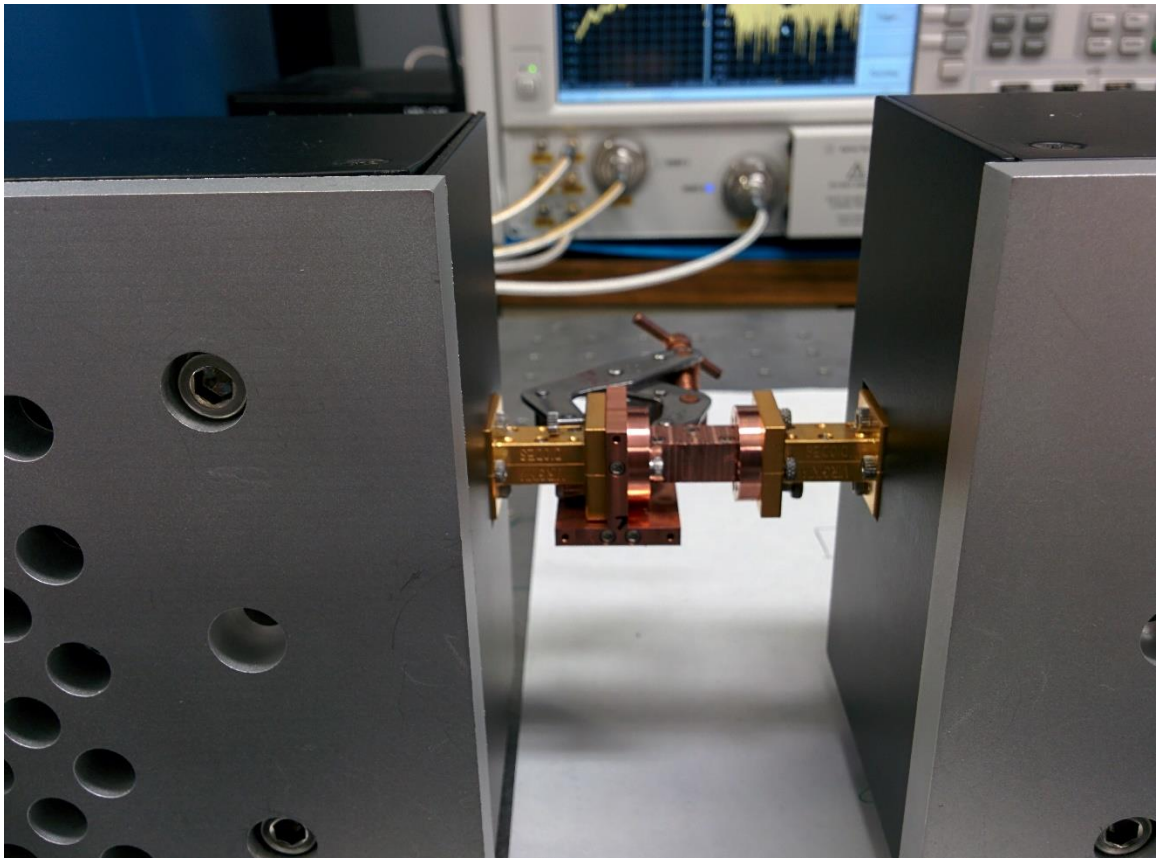

49. Test set up for Pol 2 transmission measurement (Through arm)

Pol 1 transmission measurement set up is shown in the picture below. The extension heads are positioned perpendicular each other. The side arm output of the OMT is connected to WR1.0 waveguide port of the analyzer through a straight section of WR1.0 employing UG387 flange. The through arm waveguide of the OMT was terminated with a matched WR1.0 waveguide load.

Due to the geometry of the OMT output ports and the test set up, isolation parameter was not measured.

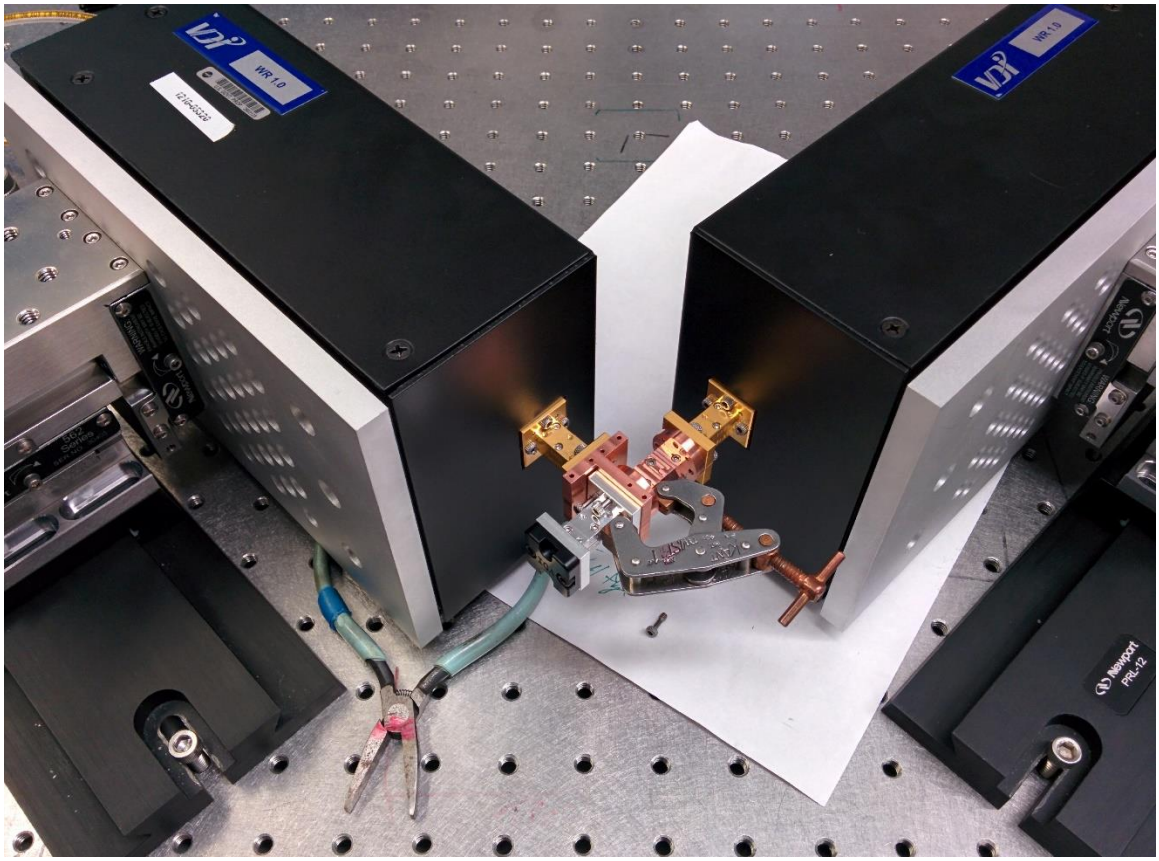

50. Test Set up for Pol 1 transmission measurement (Side arm)

7.3 Test Results

The two port S parameter response of the calibrated device set up is given below:

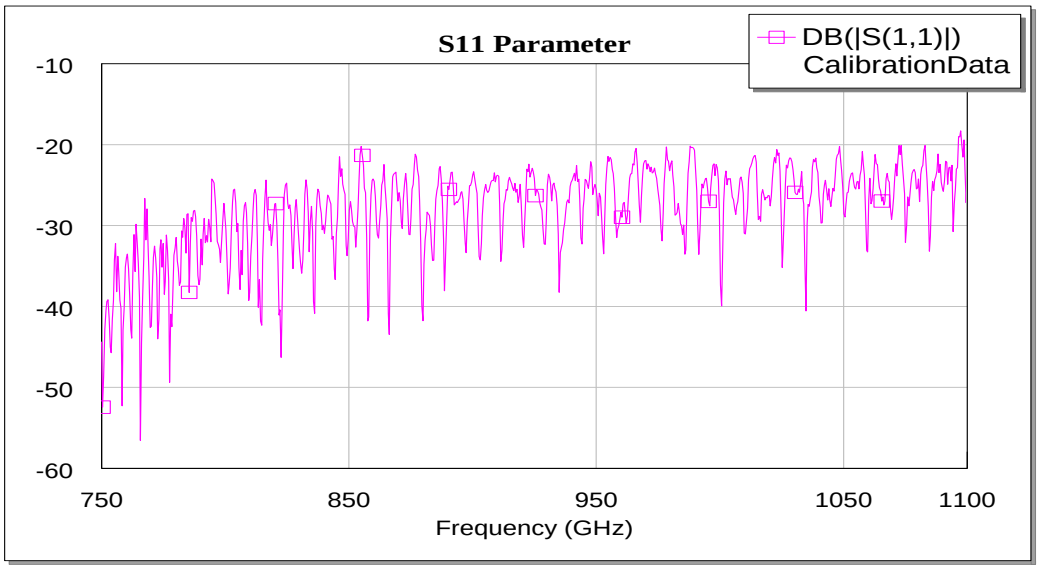

51. Calibration Data- S_{11} Parameter

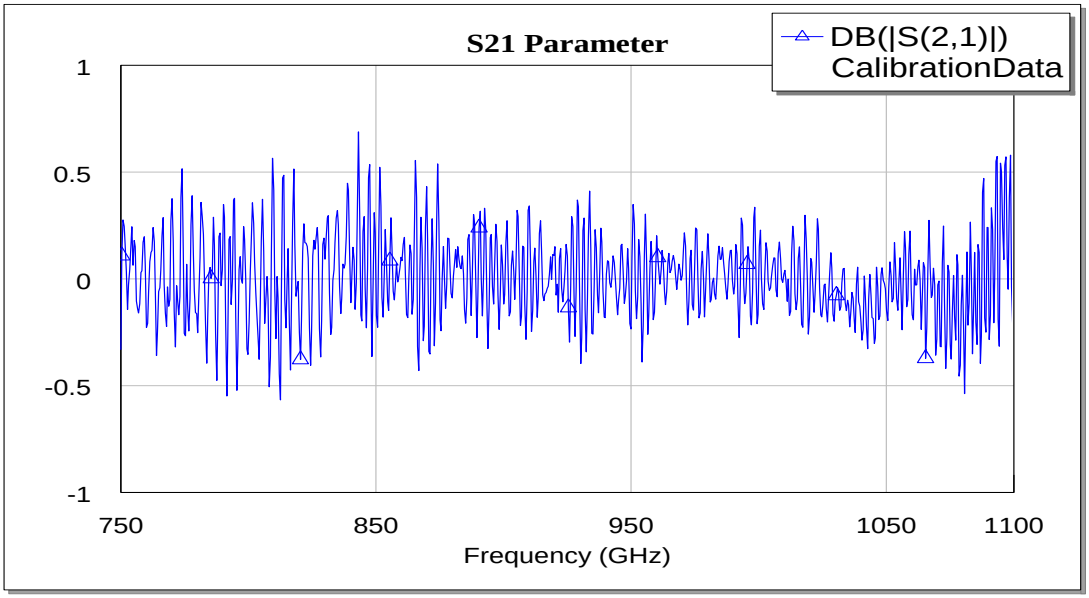

52. Calibration Data- S_{21} Parameter

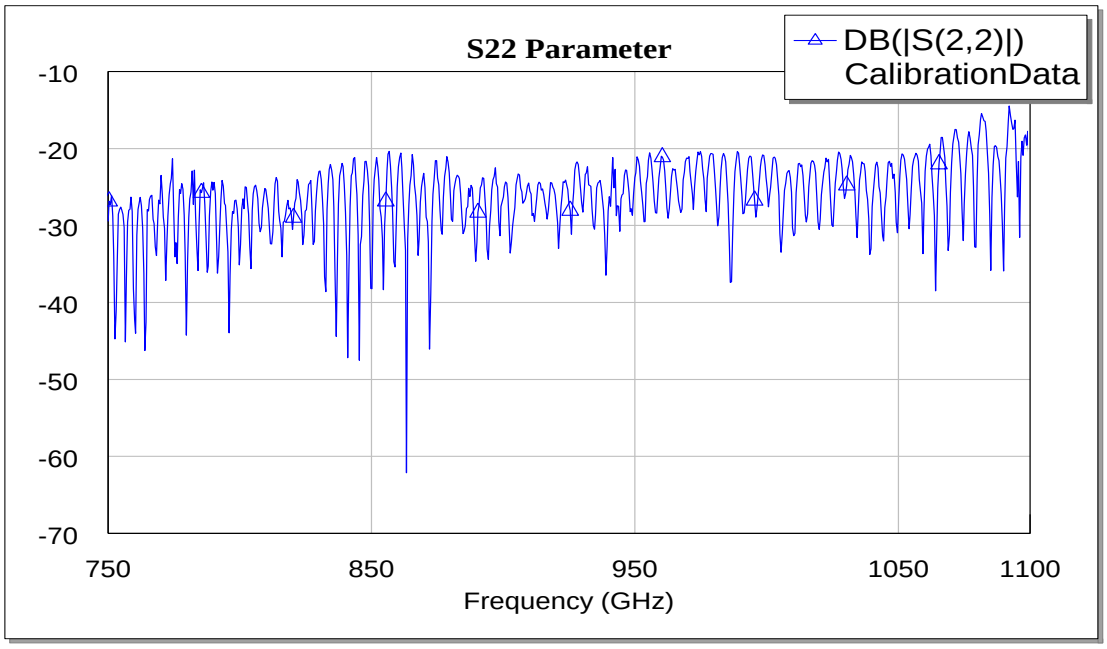

53. Calibration Data- S_{22} Parameter

The two port S parameter response for the back to back rectangular to square transition is given below:

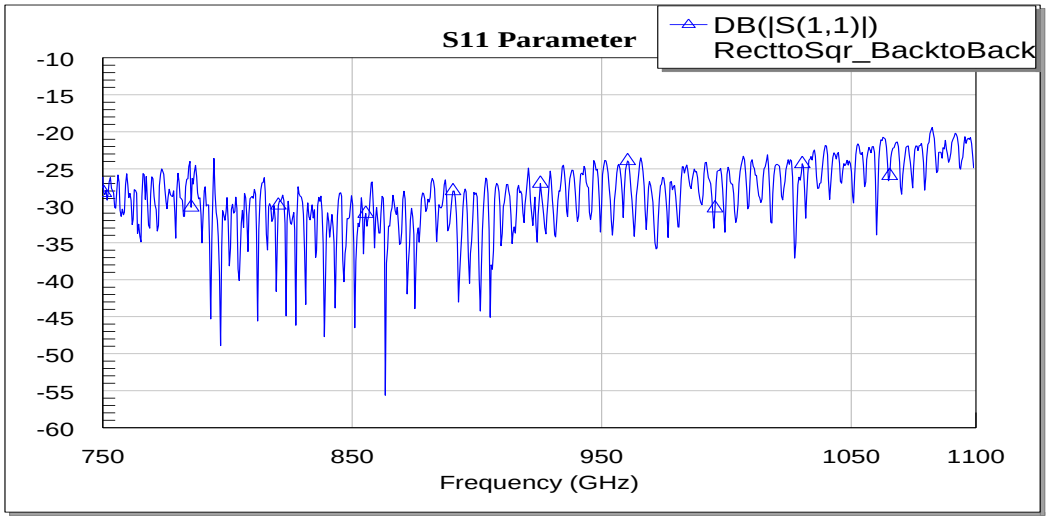

54. Return loss for back to back rectangular to square transition

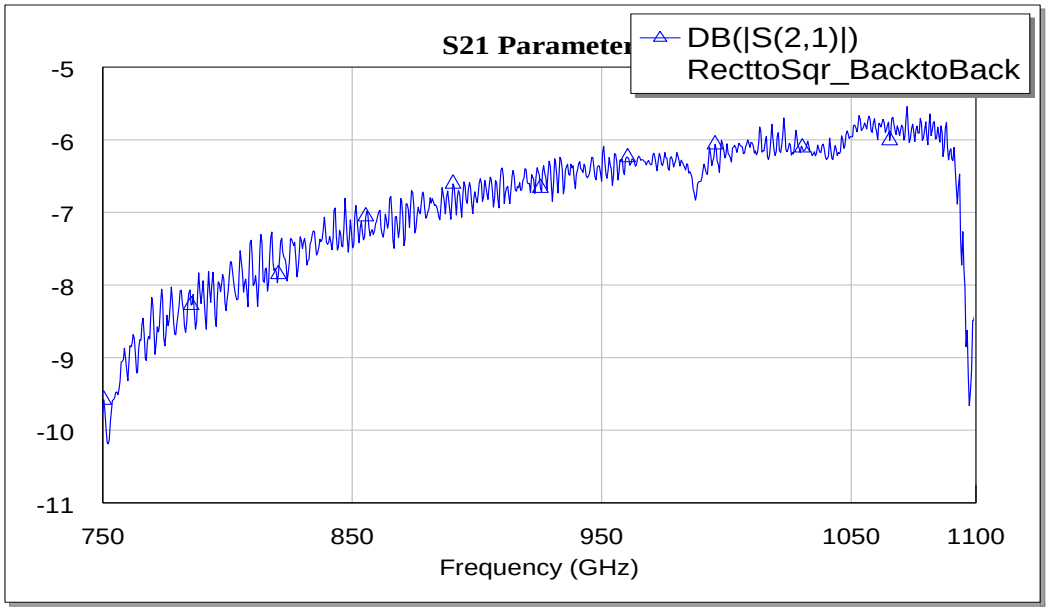

55. Insertion loss for back to back rectangular to square transition

The two port S parameter response for Pol 2 transmission (through arm) for the large chip model is given below:

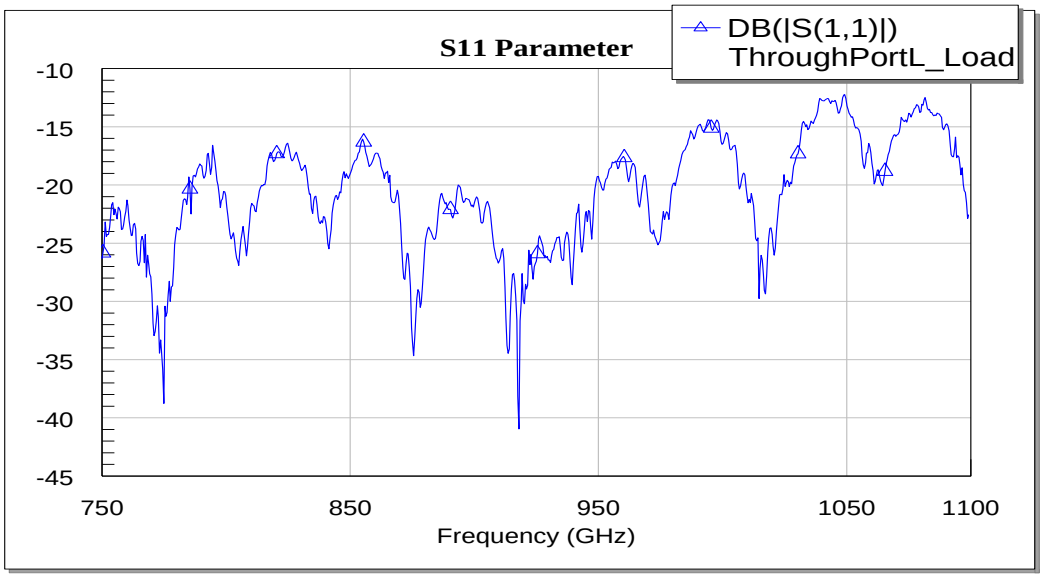

56. Return Loss for through arm- Large Chip OMT

The insertion loss measured includes the 3 dB loss introduced by a single linear rectangular to square waveguide transformer at the input of the OMT. Hence the actual loss is 3 dB less than the measured values.

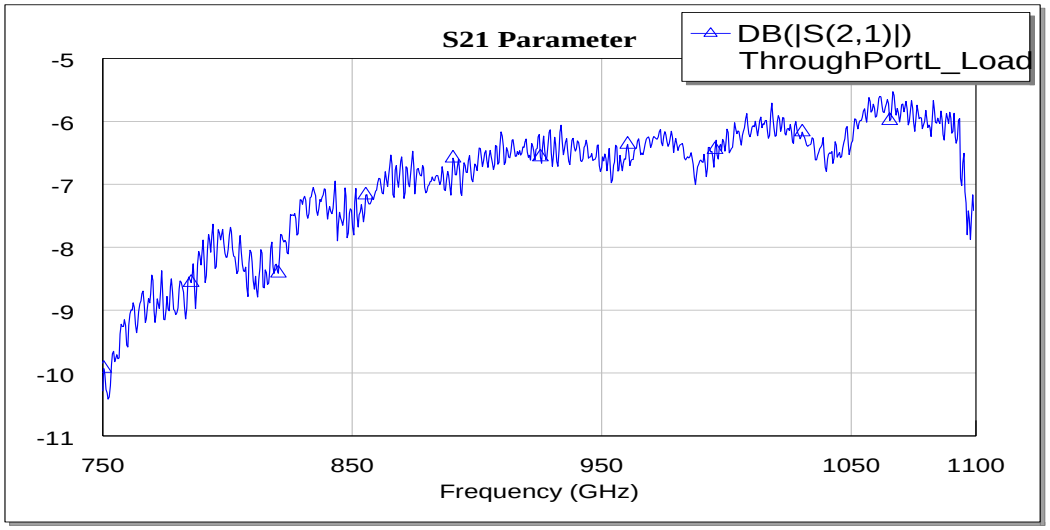

57. Insertion Loss for through arm- Large Chip OMT

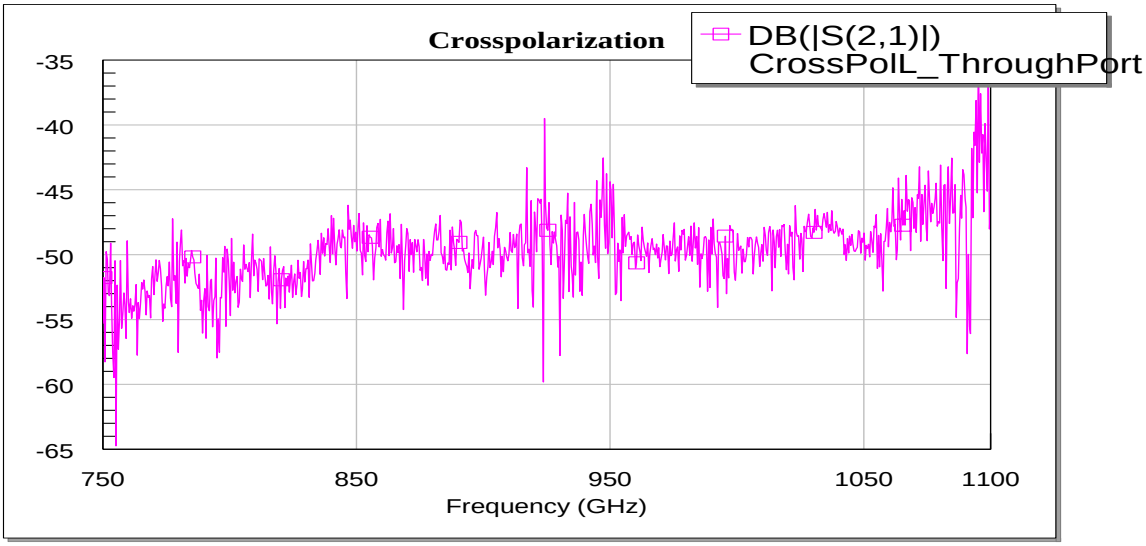

58. Crosspolarization for through arm- Large Chip OMT

The two port S parameter response for Pol 1 transmission (side arm) for the large chip model is given below:

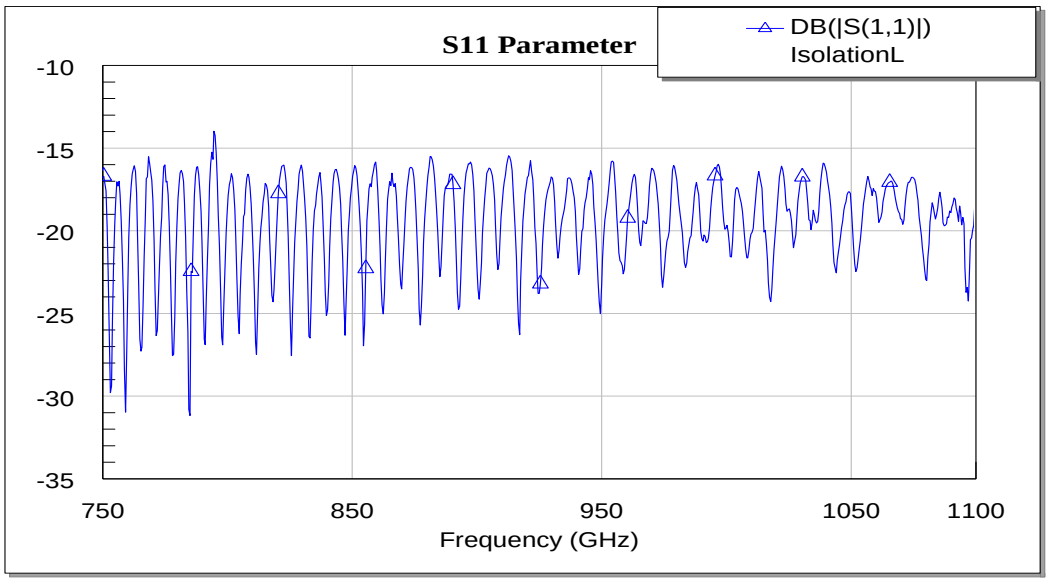

59. Return loss for side arm- Large Chip OMT

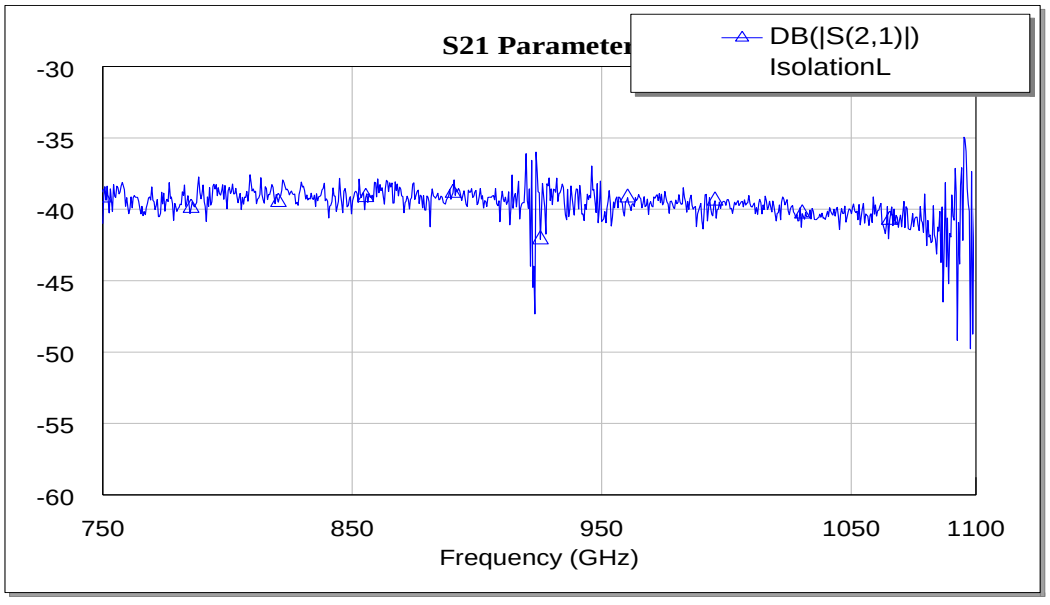

60. Insertion Loss for side arm- Large Chip OMT

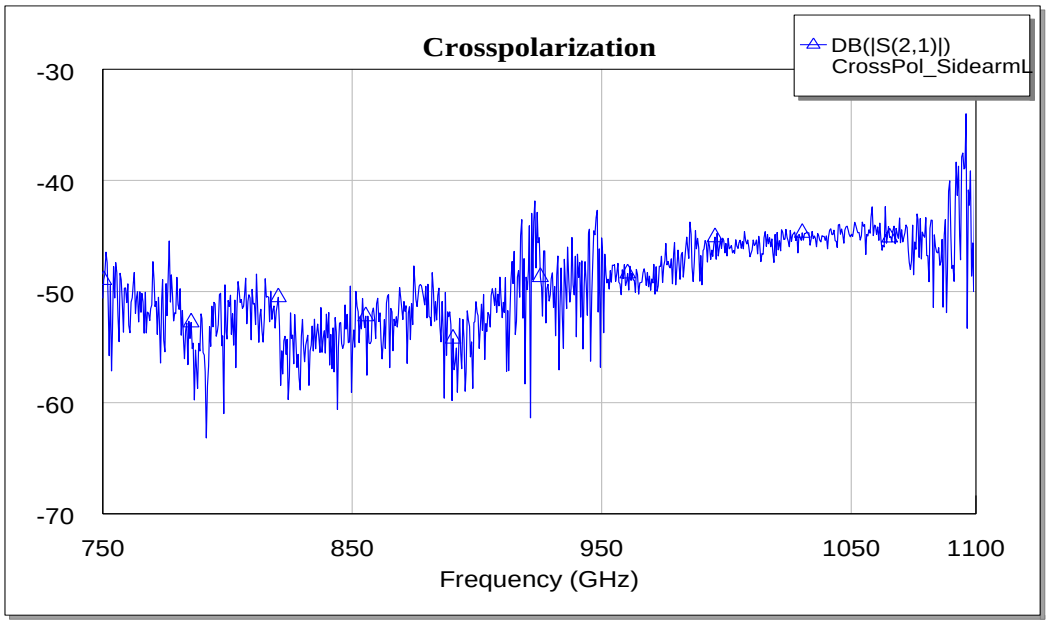

61. Crosspolarization for side arm- Large Chip OMT

The two port S parameter response for Pol 2 transmission (through arm) for the small chip model is given below:

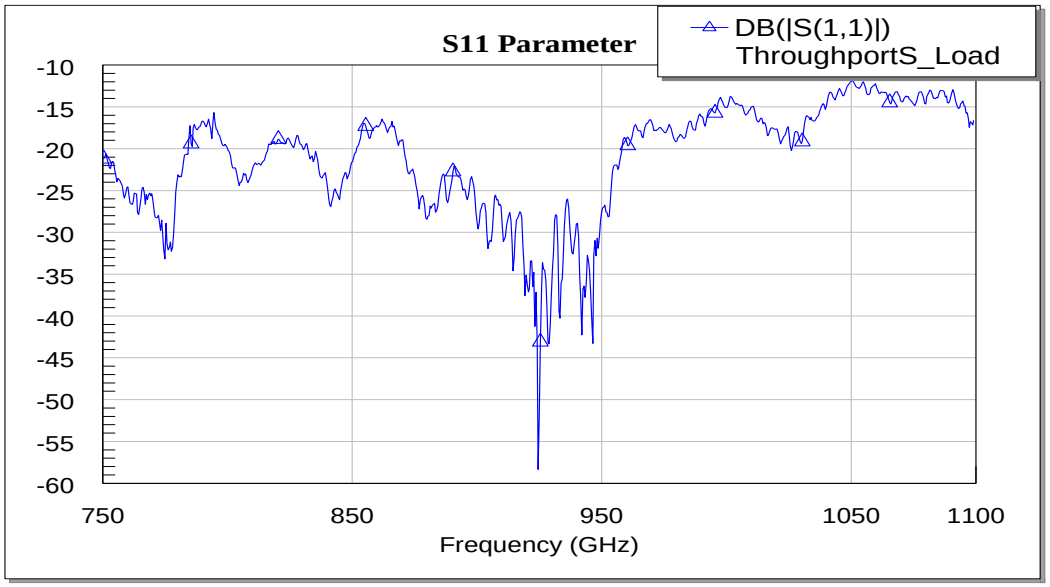

62. Return loss for through arm- Small Chip OMT

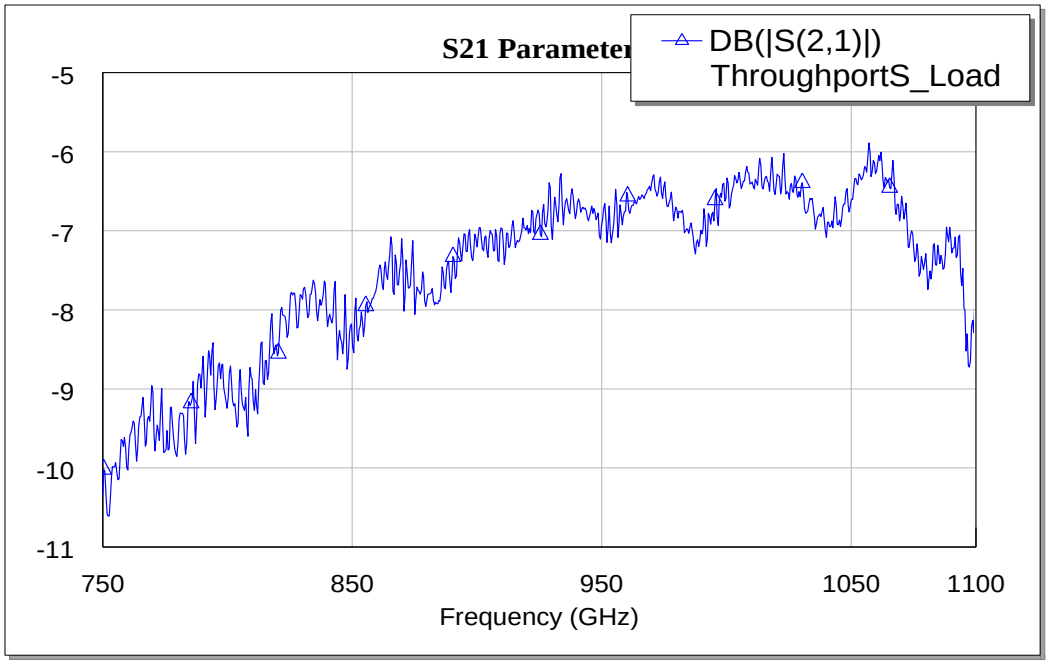

63. Insertion loss for through arm- Small Chip OMT

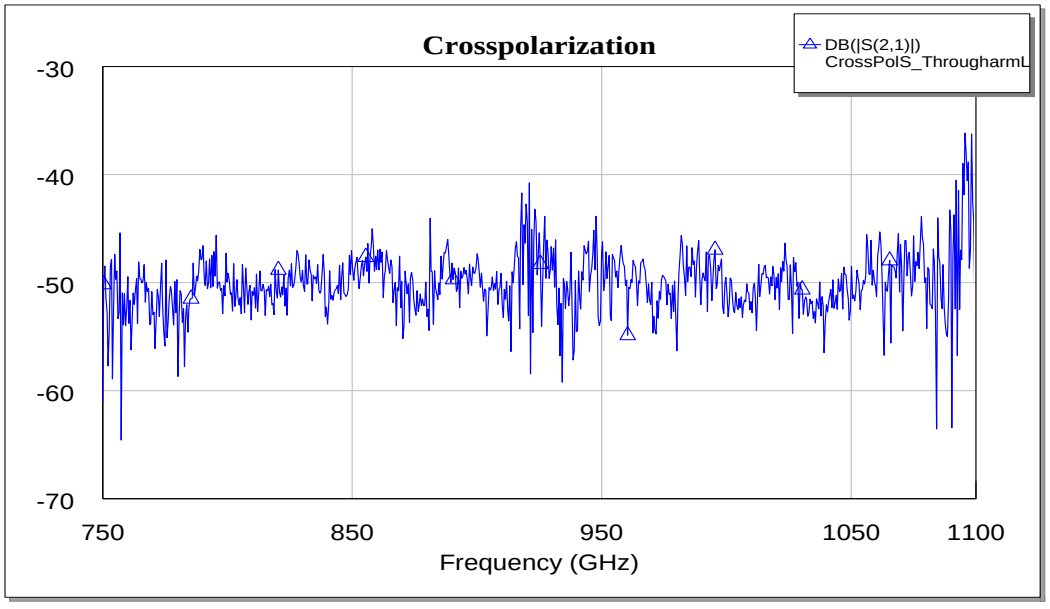

64. Crosspolarization for through arm- Small Chip OMT

The two port S parameter response for Pol 1 transmission (side arm) for the large chip model is given below:

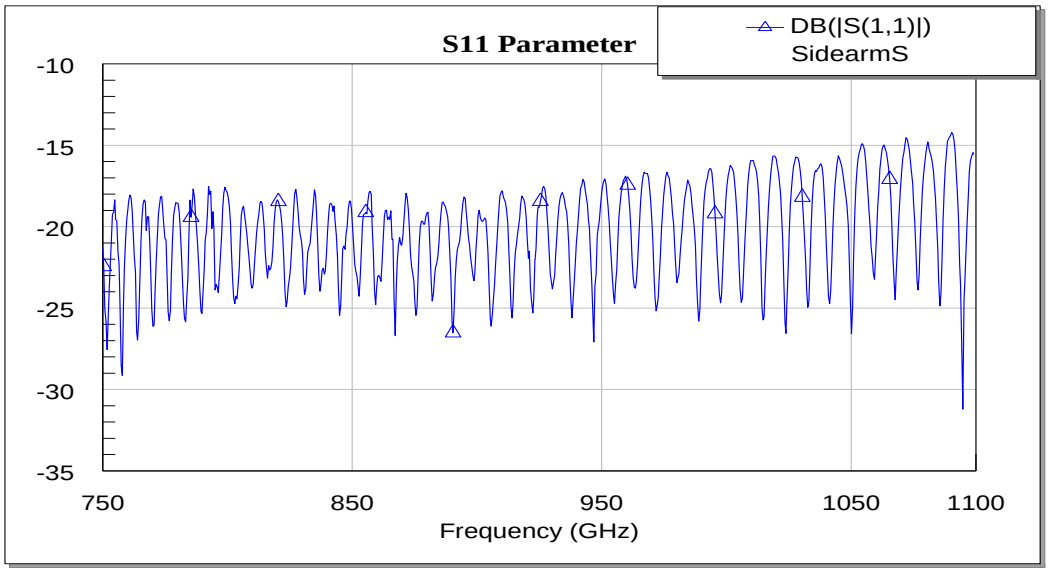

65. Return loss for side arm- Small Chip OMT

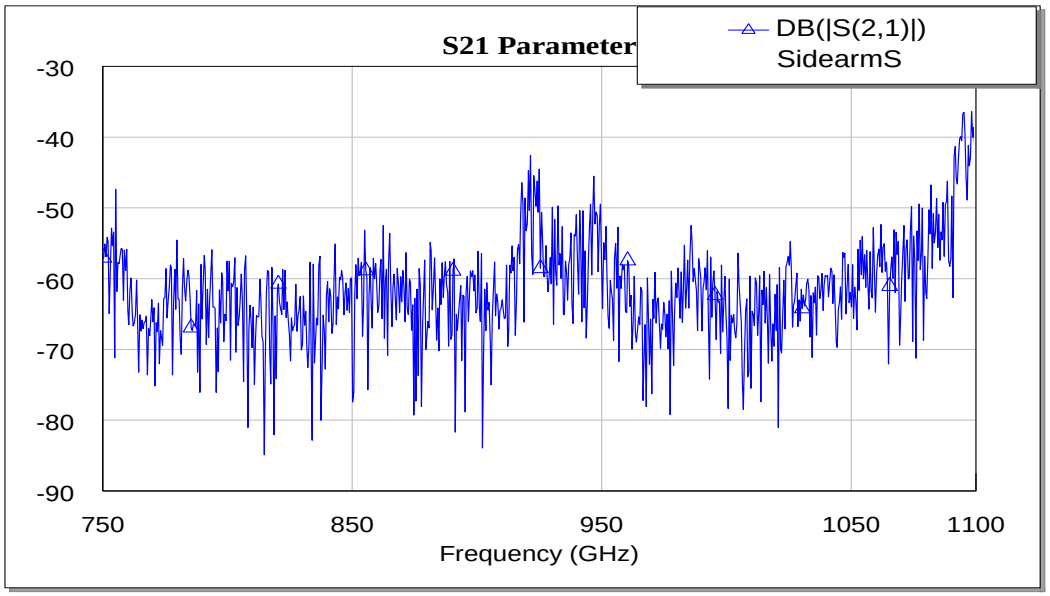

66. Insertion loss for side arm- Small Chip Model

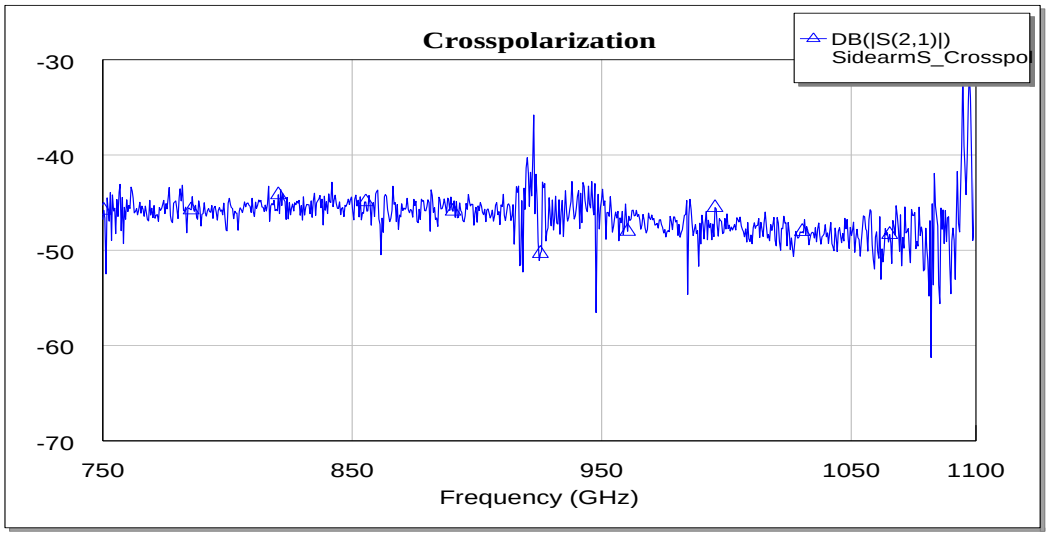

67. Crosspolarization for side arm- Small Chip Model

7.4 Comparison between simulated and observed results

The test results for the large chip model compared against the simulated response is given below. Pink colour represents the simulated results and blue represents observed results.

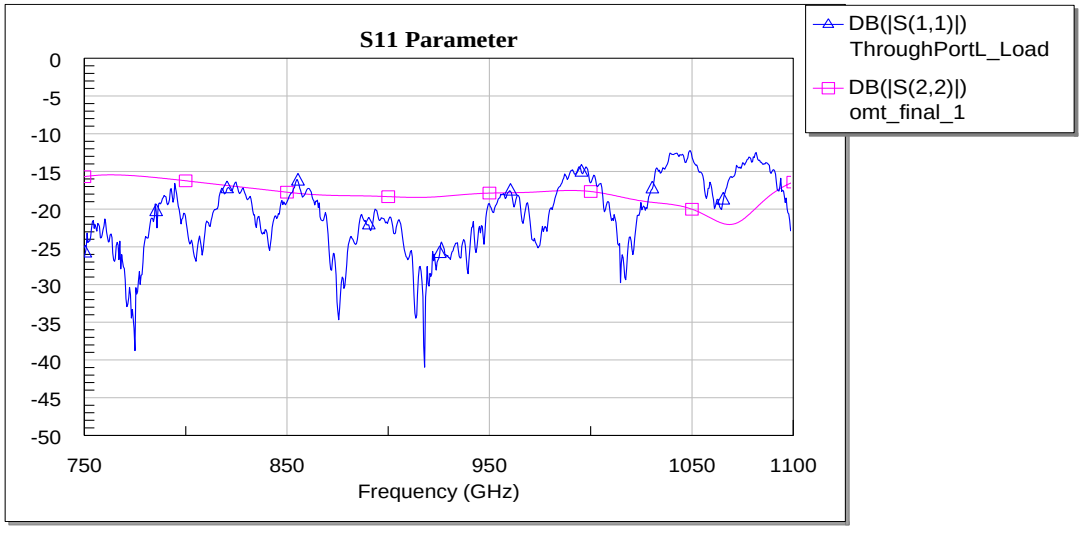

68. Return Loss- Through arm

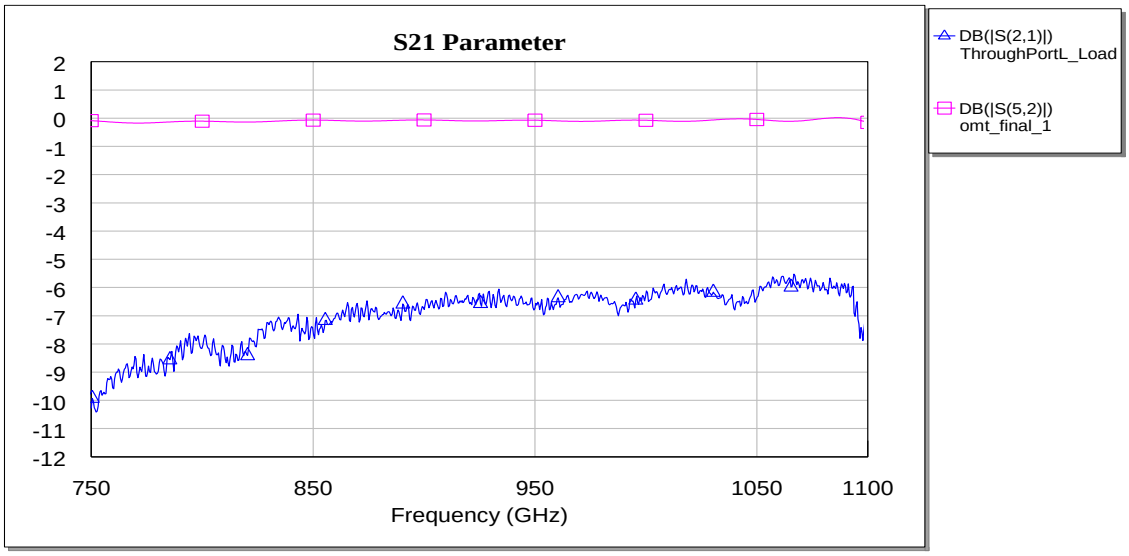

69. Insertion Loss- Through arm

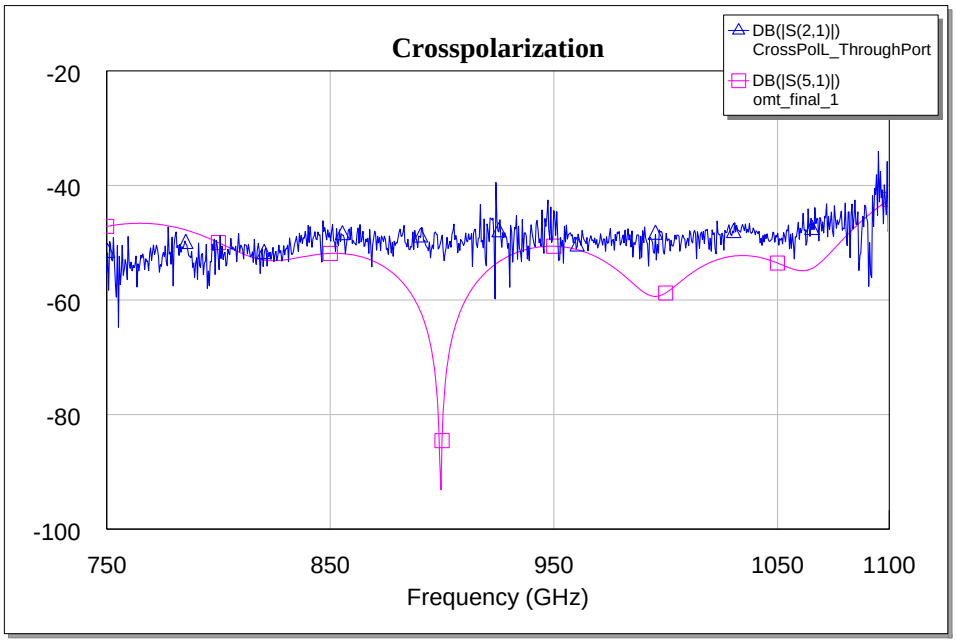

70. Crosspolarization- Through arm

The plots for return loss and crosspolarization show good agreement between the simulated and observed results. The plots for the insertion loss shows a mismatch of around 6 dB. Factoring in the 3 dB loss due to the rectangular to square transformer, the mismatch is reduced to 3 dB. This can be attributed to the ohmic losses associated with copper since a perfect electrical conductor (PEC) is considered during simulation.

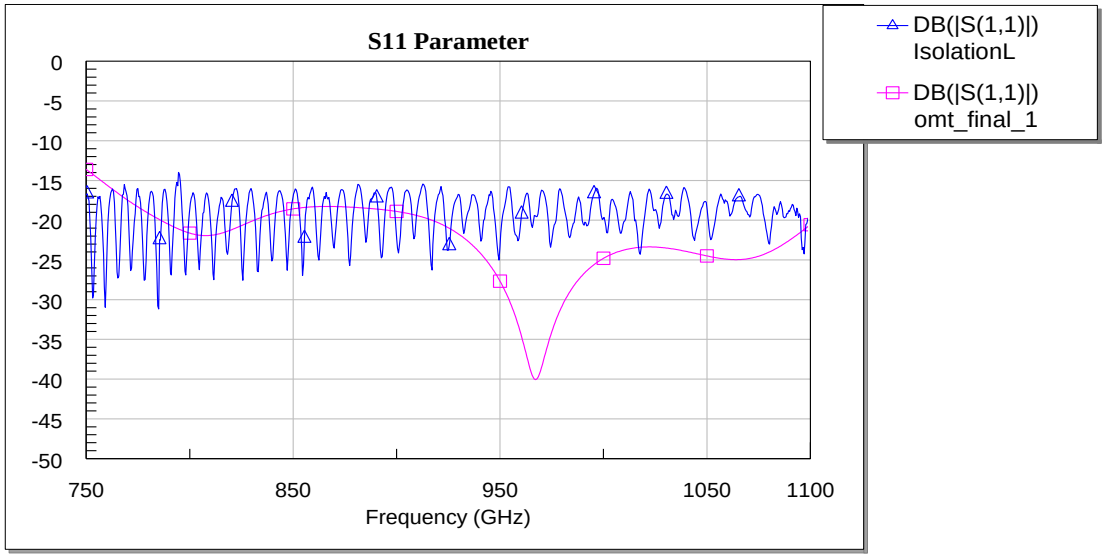

71. Return Loss- Side arm

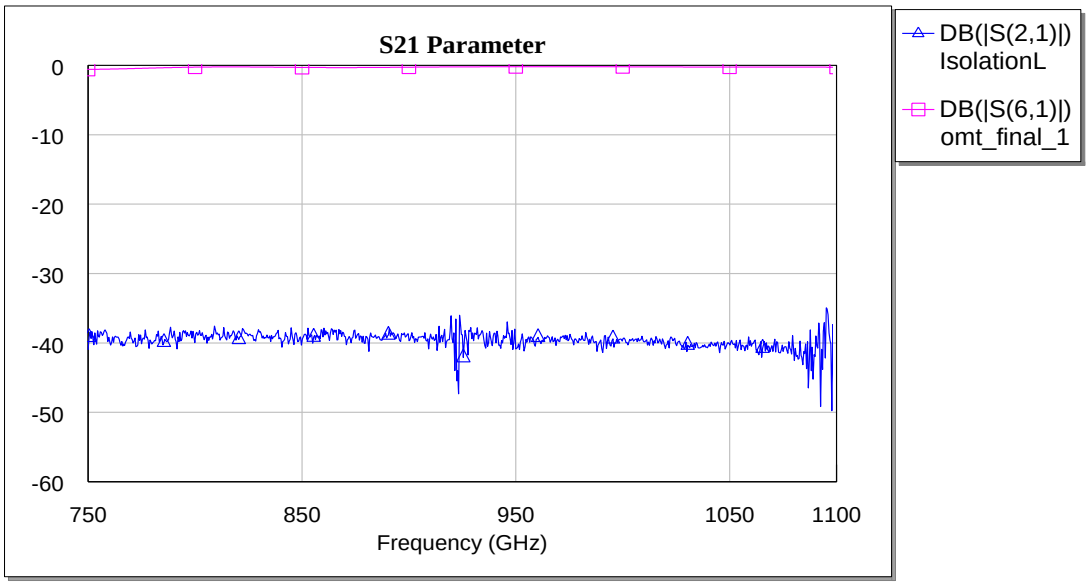

72. Insertion Loss- Side arm

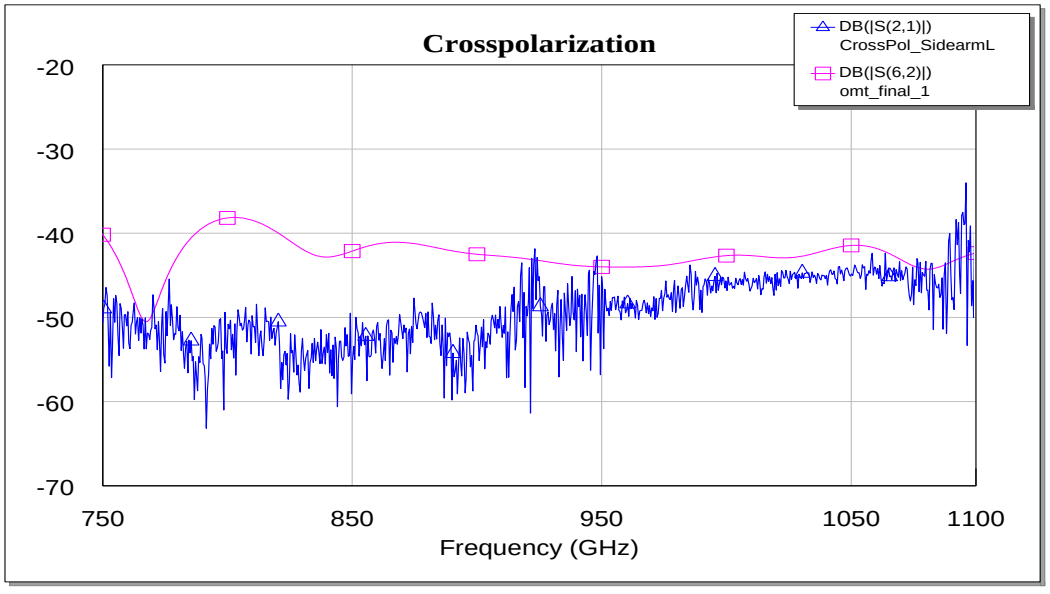

73. Crosspolarization- Side arm

There is good agreement between the simulated and observed results for the return loss and crosspolarization. The Insertion loss shows a large mismatch of around 40 dB across the bandwidth.

7.5 Side arm Insertion loss

The observed 40 dB mismatch in the side arm insertion loss can be attributed to the low resistivity of the silicon substrate. The length of the side arm and the roughness of the gold plating adds an additional 3-6 dB loss. But the main contribution is from the substrate loss.

Re-running the simulation after factoring the low resistivity of silicon, 0.2 Ω-cm or 500 S/m yields reasonable match between the observed and simulated result. At 0.5 Ω-cm resistivity, a drastic reduction in insertion loss is observed. At 10 Ω-cm resistivity the finline chip will meet all the pre-defined performance criteria.

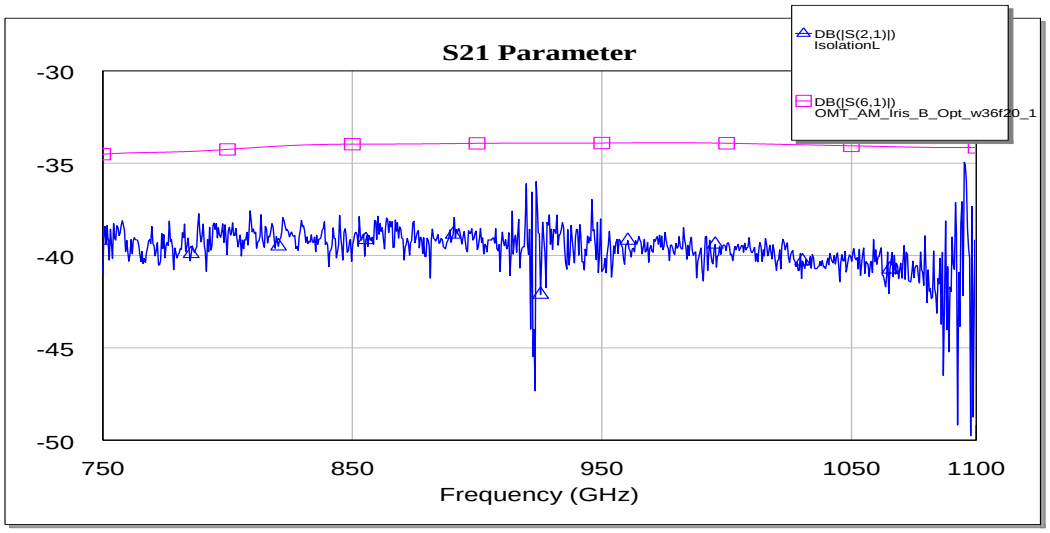

74. Comparison between insertion loss for silicon with 0.2 Ω-cm resistivity and observed result- Side arm

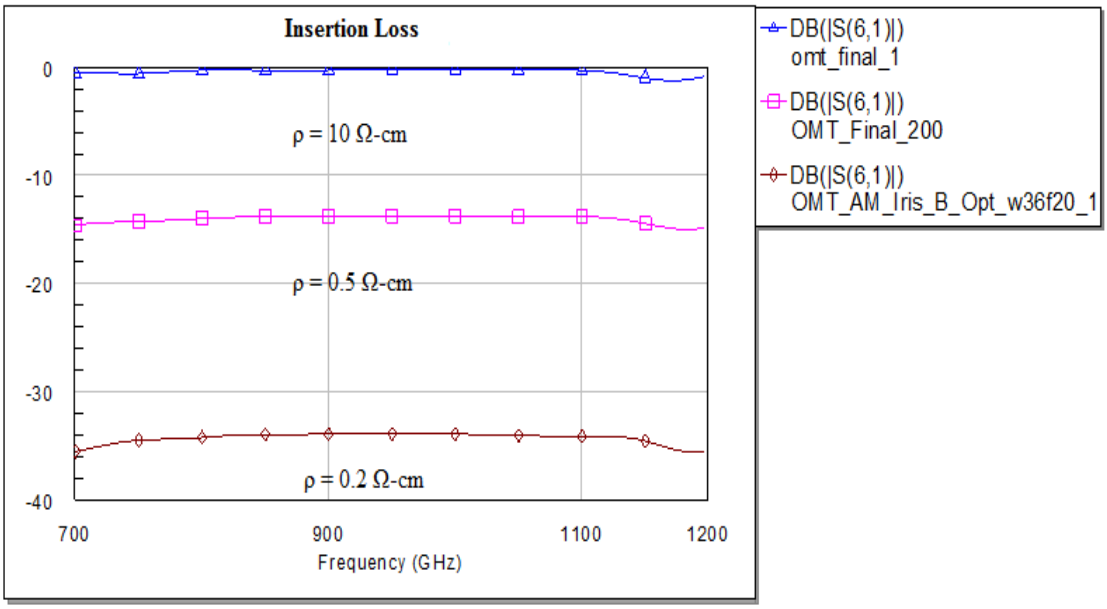

75. Insertion loss for different values of resistivity of silicon- Side arm

To test the substrate loss theory for the side arm insertion loss, the DC resistance of the finline chip was measured. The resistance of the chip was measured at room temperature and then at 77 K. The resistance increased from 19.8 Ω to 22.48 Ω. This 2 Ω increase in resistance was seen in all the trials performed. The fact that the resistivity goes up at all is clear evidence that the silicon resistivity is not high.

8. Conclusion

A 40% bandwidth orthomode transducer capable of operation from 750-1150 GHz is designed and fabricated. The design is fully planar and employs the model first proposed by Robinson in 1956 along with a planar finline circuit. The OMT is designed around the existing finline chips. Design features to accommodate for the use of standard micromilling techniques are incorporated. Various transition designs for the through arm are investigated. The waveguide iris junction between the through arm and the side arm of the OMT is designed and optimized to improve the response of the side arm. Simulation results comply with the previously set performance criteria. The OMT is fabricated using standard CNC micromachining technique. Testing of the OMT is carried out at Jet Propulsion Lab using Agilent PNA X VNA along with VDI WR1.0 extension heads. The observed result is in good agreement with the simulated result for the through arm performance. The mismatch between the expected and observed result for the side arm response is due to the low resistivity of the silicon substrate.

In the future, the finline chips can be fabricated using high resistivity silicon. Also, design changes such as etching away the silicon around the narrow region of the finline bend can be investigated. The design is scalable to frequencies as high as 5 THz. A 40% increase in the speed of signal processing can be achieved in Radio Astronomical applications with the use of this design.

REFERENCES

[1] Christopher E. Groppi, Christian Y. Drouet d'Aubigny, Arthur W. Lichtenberger, Christine M. Lyons, Christopher K. Walker, "Broadband Finline Ortho-Mode Transducer for the 750-1150 GHz Band," ISSTT Proceedings.

[2] H. Schlegel and W.D. Fowler, "The ortho-mode transducer offers a key to polarization diversity in EW systems'" Microwave System News, September 1984, pp. 65-70.

[3] A.M. Bøifot, E. Lier, T. Schaug-Pettersen, "Simple and broadband orthomode transducer," IEEE Proceedings, Vol. 137, Pt. H, No.6, December 1990

[4] J.R Brian, "The design and evaluation of a high performance 3 m antenna for satellite communication," The Marconi Review, 1978, Fourth Quarter, pp. 218-236

[5] E.J. Wollack, W. Grammer, & J. Kingsley, "The Bøifot orthomode junction," ALMA memo #425, 2002.

[6] E.J. Wollack & W. Grammer, "Symmetric waveguide orthomode junctions," 14th International Symposium on Space Terahertz Technology, University of Arizona, 2003, pp. 169.

[7] G. Narayanan & N.R. Erickson, "A novel full waveguide band orthomode transducer," 13th International Symposium on Space Terahertz Technoogy, Harvard University, 2002.

[8] G. Narayanan & N.R. Erickson, "Full-waveguide band orthomode transducer for the 3mm and 1mm bands," 14th International Symposium on Space Terahertz Technology, University of Arizona, 2003, pp. 508.

[9] S.D. Robinson, "Recent advances in finline circuits," IRE Trans, MTT, vol. MTT-4, 1956, pp. 263.

[10] S.J Skinner and G.L James, "Wide-band orthomode transducers," IEEE Trans. Microwave Theory Tech., vol.39, pp. 294-300, Feb, 1991.

[11] David M. Pozar, "Microwave Engineering," Fourth Edition

[12] G. Chattopadhyay & J.E. Carlstrom, "Finline ortho-mode transducer for millimeter waves, IEEE Microwave and Guided Wave Let., vol. 9, no. 9, 1999, pp. 339.

[13] S.J. Skinner & G.L. James, "Wide-band orthomode transducers," IEEE MTT, vol. 39, no.2, 1991, pp. 294.

[14] C.E. Groppi, C.Y. Drouet d'Aubigny, A.W. Lichtenberger & C.K. Walker, "A broadband finline ortho-mode transducer for THz applications," 15th International Symposium on Space Terahertz Technology, University of Massachusetts, 2004, pp. 314.

[15] G. Narayanan, N.R. Erickson & R.M. Grosslein, "Low cost direct machining of terahertz waveguide structures," 10th International Symposium on Space Terahertz Technology, 1999, pp. 518.

[16] C.Y. Drouet d'Aubigny, C.K. Walker, D. Golish, M.R. Swain, P.J. Dumont & P.R. Lawson, "Laser micro-machining of waveguide devices for sub-mm and far IR interferometry and detector arrays," Proc. SPIE., vol. 4852, 2003, pp.568.

[17] R.B. Bass, A.W. Lichtenberger, R.M. Weikle, S.-K. Pan, E. Bryerton, C.K. Walker, "Ultra-thin silicon chips for submillimeter-wave applications," 15th International Symposium on Space THz Technology, University of Massachusetts, 2004, pp. 392.

[18] R. P. Hecken, "A near-optimum matching section without discontinuities," IEEE Trans. Microwave Theory Tech., vol. MTT-20, pp. 734–739, NOV.1972.

[19] W. Grammer, "Design of a Near-Optimum Waveguide Taper Transition," Electronics Division Technical Note No.182, NRAO, JAN14-1998.

[20] Christopher E. Groppi, Brian Love, Matthew Underhill, Christopher Walker, "Automated CNC Micromachining for Integrated THz Waveguide Circuits," 21st International Symposium on Space Terahertz Technology, Oxford, 23-25 March, 2010

[21] Alessandro Navarrini, Christopher Groppi, Robert Lin and Goutam Chattopadhyay, "Test of a Waveguide Orthomode Trasducer for the 385-500 GHz Band," 22nd International Symposium on Space Terahertz Technology, Tuscon, 26-28 April, 2011

[22] A. Dunning, S. Srikanth and A.R. Kerr," A simple Orthomode Transducer for Centimeter to Submillimeter Wavelengths," International Symposium on Space Terahertz Technology, April 2009